1993

A biomechanical study of the fifth metatarsal

Sean McIntyre
Lehigh University

AUTHOR:

McIntyre, Sean

TITLE:

A Biomechanical Study of the Fifth Metatarsal

DATE: October 10, 1993

A BIOMECHANICAL STUDY OF THE FIFTH METATARSAL

by
Sean McIntyre

A Thesis
Presented to the Graduate Committee
of Lehigh University
in Candidacy for the Degree of
Master of Science
in
Applied Mathematics

Lehigh University
1993

This thesis is accepted in partial fulfillment of the requirements for the degree of Master of Science.

August 18, 1993
(Date)

Dr. E. Salathé
Thesis Advisor

Dr. R. Wei
Chairman, Department of
Mechanical Engineering and Mechanics

Acknowledgements

I would like to thank Dr. Salathé for this unique opportunity, Dr. Voloshin for the use of his expensive camera and computer equipment, Dr. C. Chen for the use of his numerous computer reference materials, Dr. D. Phillippy for his research in this area, Dr. Penny Smith and her husband for their coaching and support, the Mathematics Department for their tolerance, and the Graduate Student Council, which provided necessary periodic respites.

I dedicate this thesis to my late father, Barrie T. McIntyre, whose support helped to see me through much of this work.

Contents

List of Figures

Abstract

The main goal of this study is to develop an analytic approach to determine the stresses along the fifth metatarsal under load. Of particular interest is the study of the stress fracture known as the Jones fracture, which occurs along the midsection of the bone. To accomplish this study, a fifth metatarsal is sliced into cross sectional slides, and a digital camera takes a snapshot of each slide. Then computer software measures the slide and generates a Fourier series representation of the inner and outer boundaries of the cross section. Beam theory is used to determine the stresses within the cross section for a given force applied at the end of the bone. It is assumed that the boundaries of the cross sections are perturbed circles, and perturbation theory is used to obtain solutions for the stresses. The resulting data is generated for most of the cross sections along the bone. The next step in the project is to generate stresses for the type of force that is known to cause the Jones fracture. A statistical study of several bones is required to obtain more conclusive results about the biomechanical nature of the stresses that eventaully cause such a fracture.

Chapter 1

Introduction

The Jones fracture is a stress fracture that occurs near the insertion of the peroneus brevis adjacent to the the base of the fifth metatarsal [1]. This fracture requires a prolonged treatment to heal. The occurence of the injury depends on the orientation of the foot, and the fracture always occurs at approximately the same region of the bone. In an attempt to better understand the Jone's fracture, a biomechanical model of the fifth metatarsal was developed mathematically by Dr. D. Phillippy as part of his doctoral dissertation [2]. The objective of that model is to determine the stress distribution throughout any cross section of the fifth metatarsal in terms of the external forces and moments acting on it. The model developed is also general enough to be applied to any long bone under similiar conditions.

The fifth metatarsal can be regarded as a cantalever beam with a force applied at its head. Using beam theory from De Veubeke [3], given the external forces on the bone, the stresses and strains anywhere along the bone can be predicted. To test the model, Phillippy [2] determined the stresses in one cross section. The theory developed by Phillippy requires the cross section of the bone to be represented

analytically by a finite Fourier series. The method he used was painstaking, and required measuring by hand the radius of the bone as a function of the angle. The analytic procedure requires the coordinate center to be at the centroid of the series representation of the boundary, which was found using an iterative process, the procedure needed to be repeated several times for every cross section to be studied.

Although the mathematical model had been created, there had not been an exhaustive study applying the model to actual bones. Since there are at least 30 cross sectional slides to be analyzed for each metatarsal, Phillippy's experience with hand calculations indicated that there needed to be a more efficient way to use the model. Accordingly, one of the goals of this thesis was to computerize the process by which the cross sections are represented analytically by finding a way for the computer to automatically, recognize and measure the bone given any cross sectional slide.

The image processing software system developed in this thesis consists of several steps, starting with the appropriate lighting setup and ending with the Fourier series representation of the cross section. In the first step, diffuse light is projected through the cross sectional slide to the digital camera. Then a still picture of 256 shades of grey is taken of the slide and stored in memory. Within the picture, the edges of the bone are enhanced by several image processing techniques, the most crucial being convolution, light density histogram and direct editing of groups of pixels. After application of these functions, the inner and outer edges of the bone are highlighted and easy to identify. Completed lists of numbers which represent discrete points for each of the edges are then stored on disk.

The final steps in the image process are calculating the center of mass and

the Fourier series. The centroid is used as the axis for representing each point on the edge in polar coordinates. The average radius of each edge is calculated, and several points along each edge are selected between intervals of the same angle. Finally, these points are stored in a file on disk to be input into the program for the mathematical analysis of stress.

After the completion of the software, the mathematical model was reviewed and the calculations were verified. The model relies on deriving solutions to different forms of the Poisson differential equation with boundary and circuit conditions. As part of this thesis, the general solution method developed by Phillippy, which consisted of obtaining the solution as an asymptotic series, was examined and rederived in a form applicable specifically to this problems considered here. Appropriate changes to the software were made to reflect the complete model.

After verifying the new model, the automated method for representing the cross sectional shapes developed here was combined with the modified program for determining the stresses in the cross section. After this was accomplished, the integrated software was used to completely analyze a single bone under a variety of loading conditions. The results of this study are documented here by graphs of stresses and strains for each cross section from experimental data explained in chapter 4 and presented in the appendix. The results, discussed in the last two chapters, should provide useful information for a better understanding of the development of the Jones fracture.

Chapter 2

Image Processing Software

2.1 Introduction

The first step in the process of modelling the bone is to place it in a block of hot soft plastic resin. After the plastic hardens, the block is sliced into thin strips along its long side. This process creates many slides, each containing a cross section. One cross sectional slide is shown in Figure 2.1. One corner of the block designates the origin of the absolute coordinate system.

The object of the image processing software is to have the computer automatically generate the Fourier series description of the boundary of the bone, given the cross sectional slide. The necessary equipment consisted of the CCD camera, one grayscale monitor, the IBM 286 PC with the DT-IRIS image buffer board, and the Microsoft C compiler. The software was written in C using procedures specific to the DT-IRIS board.

To accompany the software, guides for the use and understanding of the program were written. The User's Guide explains each step in the process, from how to set up the slide to how to generate the final Fourier series and save it to a disk. The

Programmer's Guide reviews the algorithms and method of implementation used to create the actual code.

2.2 Image Enhancement

The first step in acquiring data from the cross sectional slide is to allow the camera to see the bone using appropriate background lighting. Illumination of the cross section from behind was found to be the most effictive lighting technique. Also known as backlighting, light is projected through the slide into the camera. Blocking the light, the bone appears as a thick black outline. To accomplish backlighting, the slide sits on a stage and diffuse light is directed through the slide towards the camera. The slide is aligned with the apperature in the stage every time, to determine the global x,y coordinates of the cross section. The set up is shown in Figure 2.2.

After the lighting is arranged, the camera takes a still picture of the cross sectional slide. Similiar to a black-and-white photograph, the image consists of 256 shades of gray varying in intensity from black to white. This type of digital picture is known as a gray scale image. In computer memory the image is stored in bytes that appear on the display as an individual gray pixel for each point. The resolution of the display of the complete picture is 512 by 512 pixels. The number of pixels to an inch depends on the distance between the lens and the cross sectional slide. Each pixel also has both x and y values, which correspond to its location on the displayed image.

Since the cross section of the bone itself takes up less than one quarter of the displayed image, a smaller working area is selected. Using the smaller working area takes considerably less time and less memory than the complete image. The working

area also lets both the user and the software focus on the important section of the image.

Image enhancement is the process of modifying the picture in order to make certain aspects clearer or more focused. Several methods to make the edges of the bone distinct within the image were tested. When used in conjunction with each other, the convolution transformation, the histogram and the edit pixels functions were found to be the most effective methods.

Convolution transformation has a similiar effect to placing a filter on the camera and then taking the picture. To the computer, the filter is the application of a particular rule which changes the shade of each pixel according to the shades of the pixels around it. For example, to make the image appear more blurred one could use the average of the neighboring pixel shades to determine the final shade of each pixel. In the gray scale image, parts of the edges of the bone are defined by rough steps like the blade of a saw. As one of the transformations, this blurr convolution makes the rough edges of the bone appear smooth.

Mathematically, given the original light intensity for each pixel, $IN_a(x, y)$, the convolution transform is accomplished by the operation:

$$IN(x,y) = \left(\sum_{i=x-1}^{x+1} \sum_{j=y-1}^{y+1} IN_a(i,j) W_{i,j} \right) / \omega,$$

where $IN(x, y)$ is the new light intensity for the pixel, $W_{i,j}$ are the weights or discrete function coefficients, and ω is the normalizing factor. The more important convolution is the application of the 'mexican top-hat' function. This transformation makes apparent the areas in the image that have an abrupt change in light intensity from one pixel to the next. These areas are known as the edges of the image. The result is an outline of any edge, including the inner and outer edges of the bone.

The histogram function creates a statistical graph of the distribution of light density per pixel. The columns are each numbered by the 256 light intensity values, in increasing order. For example, the number of pixels with the shade 128 is the height of the 128^{th} column. From this information, the image is reduced to 64 shades of increasing intensity, called thresholds. Let η denote the total number of pixels in the image. Then each threshold, Λ_k, is determined mathematically by

$$S = \sum_{i=1}^{n} H_i$$

$$S > \eta\, k/64 \Rightarrow \Lambda_k = n$$

for each $0 \leq n \leq 255$ and $1 \leq k \leq 64$, where H_i is the height of the i^{th} column of the histogram. Although this method subtracts from overall resolution of light intensities, the image becomes more focused and sharper. If this is used directly after the mexican top-hat convolution transform, the edges appear distinct and highlighted.

Edit Pixels is the interactive function with which one directly modifies small sections of the image. This is mostly used to erase anomalies within the image, such as an air bubble next to the bone in the plastic. When these problems are elliminated, they do not effect the next step in the process, which is identifying the edges of the bone.

2.3 Identify Edges

After the application of all of the image enchancement methods, the edges of the bone appear highlighted. Since each pixel has both x and y coordinate values, which correspond to its location on the image, identifying an edge of the bone consists of

finding all the (x, y) coordinates which comprise the edge.

Although the edges are highlighted, the light pixels that comprise the edge of the bone are made up of many intensities. One must decide which shades are consistent with those of the edge. To accomplish this, the Blackout function was created. With this function, one picks out all the shades that comprise the edge and makes them all the same intensity, *ie.* black.

The first part of identifying the edge of the bone is deciding where to start looking for that edge within the image. The difficulty is that there are usually more edges in the image than just those that correspond to the boundaries of the bone. Once the edge has started to be identified, the next part of the algorithm is to pretend that one is standing on that edge, and then walks along the edge. This continues until the edge ends or one comes back to where one started. Then pixel coordinates corresponding to the inner and outer edges of the bone are automatically recorded in lists in memory. These values are subtracted from the pixel values of the absolute x and y axes. To represent actual discrete points comprising the edge of the bone, these values are multiplied by the ratio of pixels per inch. Then the lists are saved to a temporary file on disk.

2.4 Centroid & Fourier Series

The final steps in the image processing software are to find the centroid of the bone and pick out points to represent the edges as finite Fourier series. Then the centroid is used as the origin for representing the edges in polar coordinates.

Each point along the edges is translated from an (x, y) coordinate to (r, θ) polar coordinate, with origin at the centroid. Several points along each edge are selected

using intervals of the same angle. It turns out that the optimum number of points is about 36, or approximately every 10 degrees along each edge. To determine which points to choose, the algorithm examines all the points on the edge close to the degree mark, for instance

$$\varsigma - .5^{\circ} \leq bd_{i,\theta} \leq \varsigma + .5^{\circ}$$

where ς is the angle of interest and $bd_{i,\theta}$ is the θ coordinate of the i^{th} boundary element. The selected value is taken as the point with the average radius and closest to the angle of interest. The radial location of N measured points on the inner and outer boundaries are used to construct an M term Fourier series, $M < N$, for the inner and outer boundary, using the method of least squares. This yields the coefficients a_o, a_i, a_{on}, b_{on}, a_{in}, b_{in}, $n = 1 - M$ in the Fourier series representation of the outer and inner surface of the bone, given respectively by

$$r_o = a_o + \sum_{n=1}^{M}(a_{on}\cos n\theta + b_{on}\sin n\theta) \tag{2.1}$$

$$r_i = a_i + \sum_{n=1}^{M}(a_{in}\cos n\theta + b_{in}\sin n\theta)$$

The centroid of the cross section is represented by the series given by

$$x_c = \frac{a_o^2 a_{o1} - a_i^2 a_{i1}}{a_o^2 - a_i^2} \tag{2.2}$$

$$y_c = \frac{a_o^2 b_{o1} - a_i^2 b_{i1}}{a_o^2 - a_i^2}$$

The procedure is then repeated using this location as the origin, and continued until $x_c = 0$, $y_c = 0$. Using $N = 36$ points for the edge, by experimentation it was found that $M = 12$ gives the curve that best represents the shape of the cross section. The Fourier series model for the example is pictured in Figure 2.3.

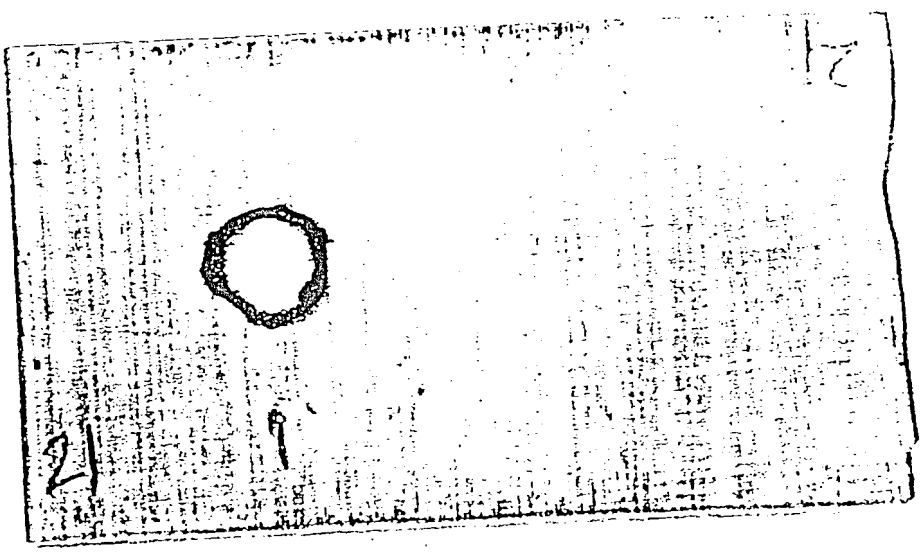

Figure 2.1: Cross sectional slide.

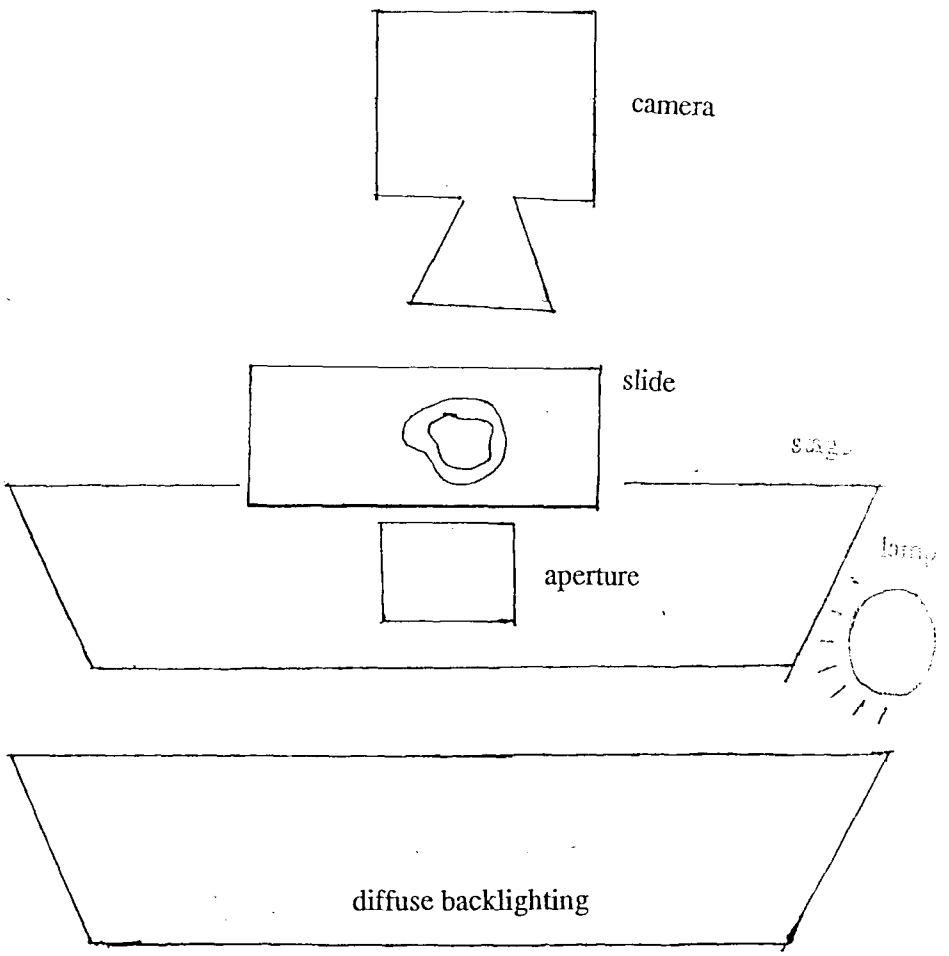

Figure 2.2: Lighting setup.

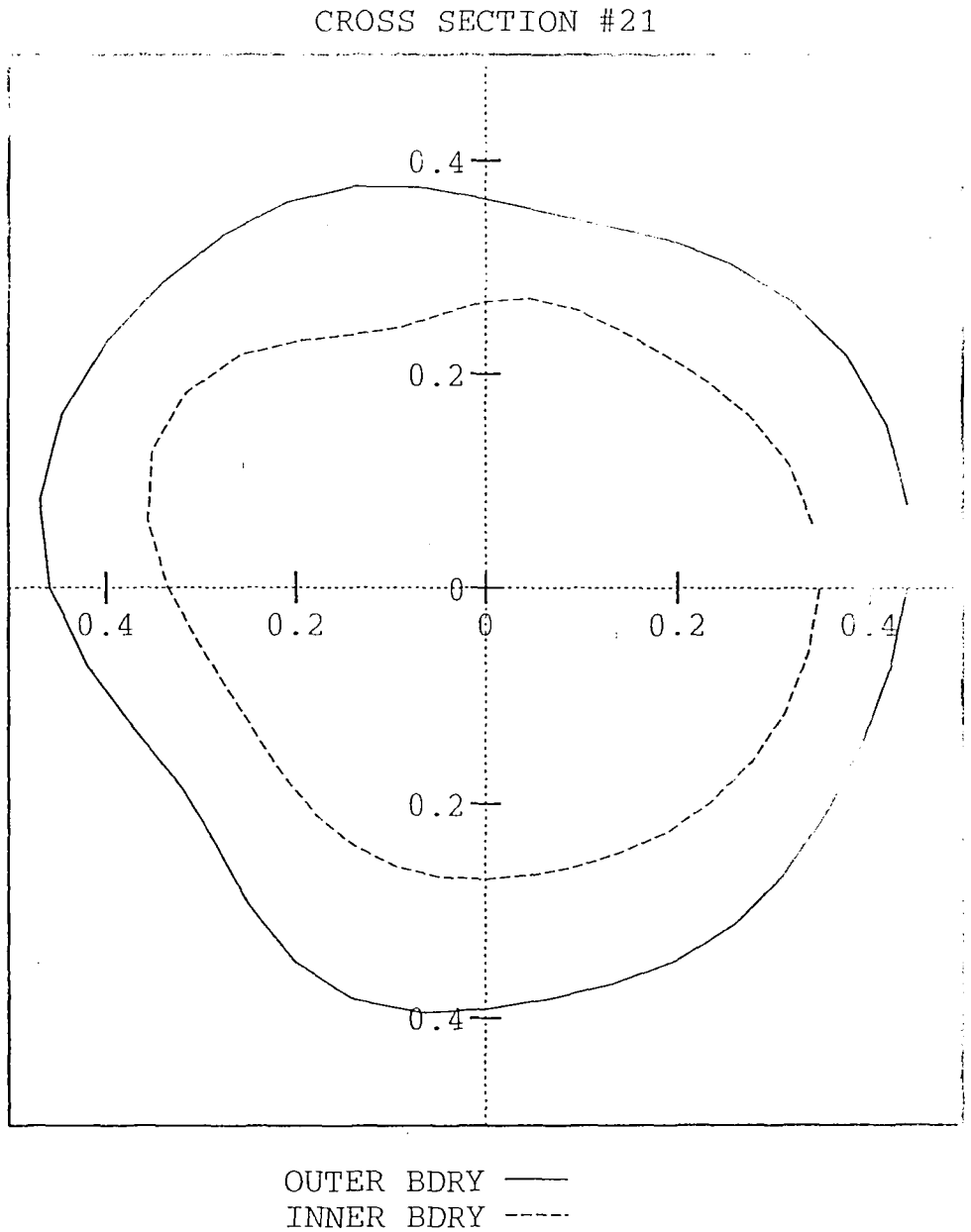

Figure 2.3: Fourier series model.

Chapter 3

Outline of Biomechanical Model

3.1 Mathematical Model of the Fifth Metatarsal

To determine the stress distribution in the bone, the properties of the cross sections of the bone are used. The cross-sectional properties are given analytically in terms of the mathematical description of the inner and outer boundaries of the bone. The stresses in any cross section are equivalent to a force $\underset{\sim}{T}$ at the centroid of the cross section and a moment $\underset{\sim}{M}$. These can readily be determined though a force and moment balance on the beam as a whole, and so are considered known at any cross section.

For each cross section, a local coordinate system is chosen with the origin at the centroid and the z-axis perpendicular to it as shown in Figure 3.1. The cross section is a doubly connected domain bounded on the outside by the circuit c_o, and on the inside by the circuit c_i. These are directed circuits, such that the tangent vector in the direction of the path, the unit vector along the z-axis, and the outward drawn normal $\underset{\sim}{n}$ form a right handed coordinate system. The outer circuit bounds an area Ω_o, the inner circuit bounds an area Ω_i, and the area of the bone is $\Omega = \Omega_o - \Omega_i$.

The force $\underset{\sim}{T}$ has components T_x and T_y along the x and y axes, respectively, called the shear forces. Along the z-axis, $\underset{\sim}{T}$ has component T_z called the axial force. The moment $\underset{\sim}{M}$ has components M_x and M_y along the x and y axes, respectively, called the bending moments. Along the z-axis, $\underset{\sim}{M}$ has component M_z called the twisting moment.

To calculate the stress distribution within a cross section in terms of the resultant force $\underset{\sim}{T}$ and moment $\underset{\sim}{M}$ at that cross section, the semi-inverse method of Saint Venant, as described by de Veubeke [3], is used. This method consists of setting

$$\sigma_x = \sigma_y = \tau_{xy} = 0$$

and seeking a solution to equations of elasticity under these conditions. The stresses to be determined are the normal stress $\sigma_z(x,y)$ and the shear stresses $\tau_{xz}(x,y)$ and $\tau_{yz}(x,y)$.

Saint Venant's method leads to the following simple solution for the normal stress in terms of the normal force T_z and bending moments M_x, M_y:

$$\sigma_z = E(K_z + xK_x + yK_y) \tag{3.1}$$

where E is Young's modulus, and K_x, K_y, K_z are given in terms of the moments and forces by

$$\begin{aligned} K_x &= \frac{I_{yy}M_x - I_{xy}M_y}{E(I_{xx}I_{yy} - I_{xy}^2)} \\ K_y &= \frac{I_{xx}M_y - I_{xy}M_x}{E(I_{xx}I_{yy} - I_{xy}^2)} \\ K_z &= T_z/(E\Omega) \end{aligned} \tag{3.2}$$

Here Ω, I_{xx}, I_{yy}, I_{xy} are the area, moments of inertia and product of inertia of the cross section.

3.1. MATHEMATICAL MODEL OF THE FIFTH METATARSAL

Determination of shear stresses τ_{xz}, τ_{yz} is a complex problem, and the procedure yeilds the shear stresses in terms of the shear forces T_x, T_y and the twisting moment M_z. This procedure requires redefining the twisting moment to allow the shear forces to act through a point in the cross section known as the center of bending-torsion denoted by the coordinates (x_F, y_F). The twisting moment about this point, M_F, is

$$M_F = M_z + T_x y_F - T_y x_F. \tag{3.3}$$

The shear stresses can be written in the form

$$\begin{aligned} \tau_{xz} &= \hat{\theta}\, G\frac{\partial \Theta}{\partial y} + E\frac{\partial \Phi}{\partial x} + G\frac{\partial K}{\partial y} \\ \tau_{yz} &= -\hat{\theta}\, G\frac{\partial \Theta}{\partial x} + E\frac{\partial \Phi}{\partial y} - G\frac{\partial K}{\partial x} \end{aligned} \tag{3.4}$$

where G is the shear modulus and $\hat{\theta}$ is the twist of the centroidial fiber due to M_F; $\hat{\theta}$ is given by

$$\hat{\theta} = M_F/(GJ) \tag{3.5}$$

where J is the torsional stiffness coefficient. The functions Θ, Φ and K are found by solving the following boundary value problems in the cross section of the bone:

$$\nabla^2 \Theta = -2 \tag{3.6}$$

$$\Theta = 0 \text{ on } c_o,\ \Theta = \alpha_i \text{ on } c_i$$

$$\oint_{c_i} \frac{\partial \Theta}{\partial n} ds = 2\Omega_i \tag{3.7}$$

$$\nabla^2 \Phi = -(Ax + By) \tag{3.8}$$

$$\frac{\partial \Phi}{\partial n} = 0 \text{ on } c_o,\ c_i$$

$$\nabla^2 \mathrm{K} = 2\nu(Ay - Bx - C) \tag{3.9}$$

$$\mathrm{K} = 0 \text{ on } c_o, \mathrm{K} = \beta_i \text{ on } c_i$$

$$\oint_{c_i} \frac{\partial \mathrm{K}}{\partial n} ds = -2\nu\Omega_i(A\hat{y}_i - B\hat{x}_i - C). \tag{3.10}$$

The circuit conditions, eqns (3.7), (3.10) assure the absense of residual stress in the doubly connected domain D, so that the stresses vanish when there are no applied loads. These conditions suffice to determine the boundary values α_i and β_i of Θ and K, respectively, on c_i. Θ gives the contribution to the shear stresses resulting from pure torsion, which depends only on the twisting moment $\mathrm{M_F}$. If the domain of Θ is extended by defining $\hat{\Theta} = \Theta$ in D and $\hat{\Theta} = \alpha_i$ in the region bounded by c_i, then

$$J = 2\int_{\Omega_o} \hat{\Theta} dx dy. \tag{3.11}$$

Φ and K are the contribution to the shear stresses resulting from bending without torsion; this contribution depends only on the shear forces T_x and T_y acting through the center of bending torsion. In terms of the shear forces, A and B are given as follows:

$$A = \frac{\mathrm{I}_{yy}\mathrm{T}_x - \mathrm{I}_{xy}\mathrm{T}_y}{\mathrm{E}(\mathrm{I}_{xx}\mathrm{I}_{yy} - \mathrm{I}_{xy}^2)} \tag{3.12}$$

$$B = \frac{\mathrm{I}_{xx}\mathrm{T}_y - \mathrm{I}_{xy}\mathrm{T}_x}{\mathrm{E}(\mathrm{I}_{xx}\mathrm{I}_{yy} - \mathrm{I}_{xy}^2)}$$

To determine the center of bending torsion $(x_{\mathrm{F}}, y_{\mathrm{F}})$, note that Φ can be broken into two parts, one depending on A and the other on B. Writing $\Phi = A\Phi_A + B\Phi_B$,

definitions for Φ_A, Φ_B follow from eqn. (3.8). Then x_{F} and y_{F} are found by solving the following equations:

$$y_{\mathrm{F}}\mathrm{I}_{xx} - x_{\mathrm{F}}\mathrm{I}_{xy} = \oint_{c_t} \Phi_A(x\,dx + y\,dy) \tag{3.13}$$

$$y_{\mathrm{F}}\mathrm{I}_{xy} - x_{\mathrm{F}}\mathrm{I}_{yy} = \oint_{c_t} \Phi_B(x\,dx + y\,dy)$$

where c_t is the total circuit consisting of both c_i and c_o. The twist of the centroidial fiber due to the shear forces acting through the center of bending torsion is νC, where ν is Poisson's ratio, and C is found from

$$C = \frac{1}{J}\left[2A\int_{\Omega_o} \hat{\Theta}\, y\, dxdy - 2B\int_{\Omega_o} \hat{\Theta}\, x\, dxdy\right]. \tag{3.14}$$

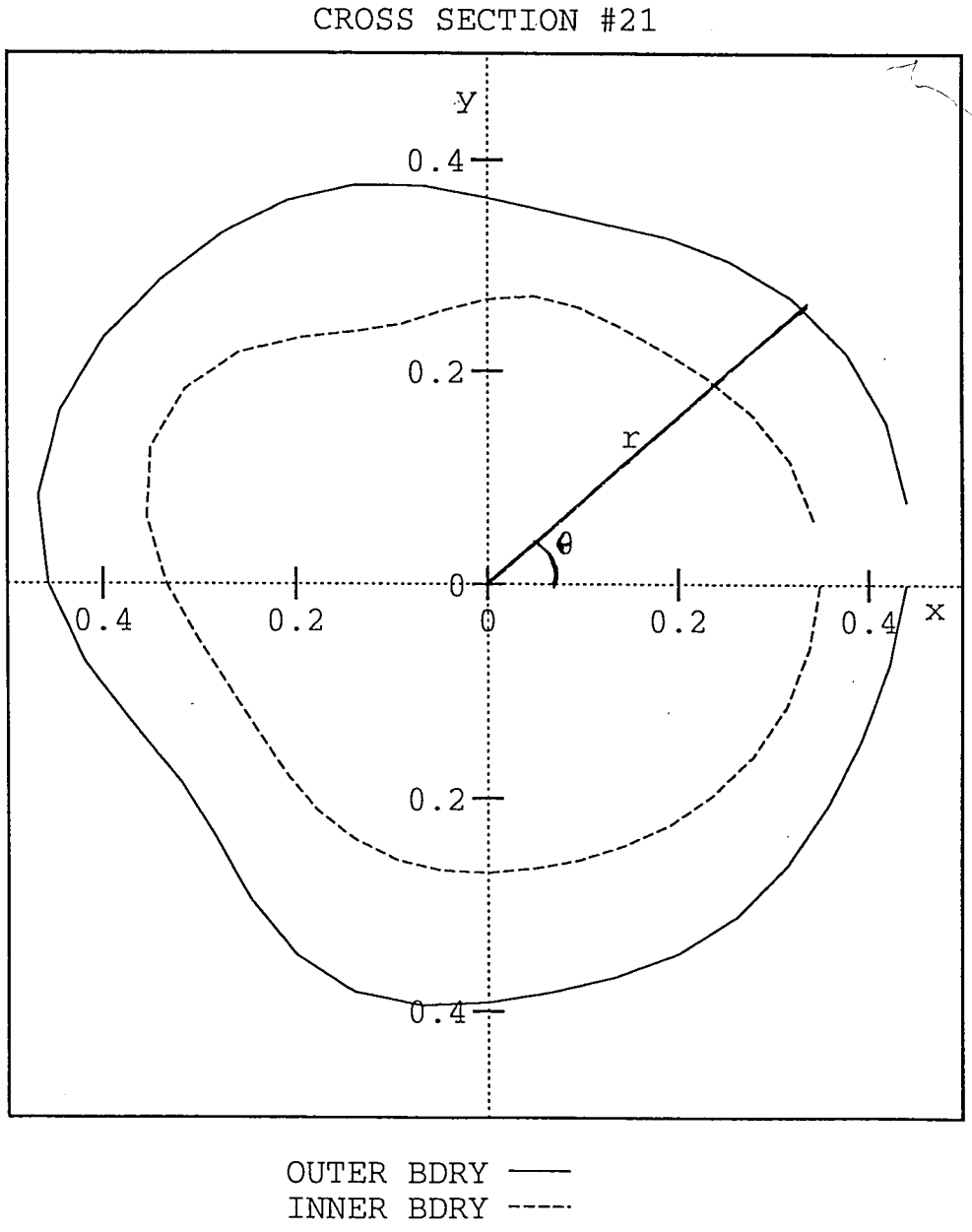

Figure 3.1: Local coordinate system of cross section.

3.2 Pertubation Analysis

3.2.1 Overview

The cross section of the bone is regarded as an annulus with small pertubations on both the inner boundary, c_0, and the outer boundary, c_i. Analytically in polar form,

$$r_0 = a_o + \epsilon f_o(\theta) \tag{3.15}$$

$$r_i = a_i + \epsilon f_i(\theta)$$

The constant terms a_o, a_i, are the mean radii of the inner and outer boundaries, respectively, ϵ is a small quantity, and both f_o and f_i have zero mean over the interval $0 \leq \theta \leq 2\pi$.

The functions Θ_0, Φ_0, K_0 correspond to the stresses in the circular annulus. The solution can be obtained as an asymptotic expansions in ϵ according to

$$\Theta = \Theta_0 + \epsilon\Theta_1 + O(\epsilon^2) \tag{3.16}$$

$$\Phi = \Phi_0 + \epsilon\Phi_1 + O(\epsilon^2)$$

$$\mathrm{K} = \mathrm{K}_0 + \epsilon\mathrm{K}_1 + O(\epsilon^2).$$

The corresponding differential equations, boundary conditions and circuit conditions for each of these functions can be derived. Since ϵ is small, it is assumed from this point onward that terms containing ϵ to a power greater than or equal to two are negligable.

A necessary part of the pertubation analysis is the expansion of the moments of inertia in terms of ϵ. First writing the moments of inertia for the annulus as $\mathrm{I} = \mathrm{I}^0_{xx} = \mathrm{I}^0_{yy}$, the asymptotic expansion of the moments and products of inertia can be written as

$$I_{yy} = I^0_{yy} + \epsilon I^1_{yy} \qquad I_{xx} = I^0_{xx} + \epsilon I^1_{xx} \qquad I_{xy} = \epsilon I^1_{xy}.$$

In terms of polar coordinates, these formulae are given by

(3.17)
$$\begin{aligned} I &= \pi(a_o^4 - a_i^4)/4 \\ I^1_{xx} &= \int_0^{2\pi} [a_o^3 f_o(\theta) - a_i^3 f_i(\theta)] \cos^2\theta \, d\theta \\ I^1_{xy} &= \int_0^{2\pi} [a_o^3 f_o(\theta) - a_i^3 f_i(\theta)] \cos\theta \sin\theta \, d\theta \\ I^1_{yy} &= \int_0^{2\pi} [a_o^3 f_o(\theta) - a_i^3 f_i(\theta)] \sin^2\theta \, d\theta \end{aligned}$$

The asymptotic expansions of the parameters K_x, K_y and K_z are needed to develop the normal stress at any point along the bone. Using the notation $K_x = K_{x0} + \epsilon K_{x1}$, $K_y = K_{y0} + \epsilon K_{y1}$ and $K_z = K_{z0} + \epsilon K_{z1}$, it is found that

(3.18)
$$K_{x0} = \frac{M_x}{EI} \qquad K_{y0} = \frac{M_y}{EI} \qquad K_{z0} = \frac{T_x}{E\pi(a_o^2 - a_i^2)}$$
$$K_{x1} = -\frac{I^1_{xy} M_y + I^1_{xx} M_x}{EI^2} \qquad K_{y1} = -\frac{I^1_{xy} M_x + I^1_{yy} M_y}{EI^2} \qquad K_{z1} = 0.$$

Therefore the expansion for normal stress, $\sigma_z = \sigma_{z0} + \epsilon\sigma_{z1}$, can be derived, in which

(3.19)
$$\begin{aligned} \sigma_{z0} &= E(K_{z0} + x\, K_{x0} + y\, K_{y0}) \\ \sigma_{z1} &= E(x\, K_{x1} + y\, K_{y1}). \end{aligned}$$

The pertubation analysis requires the coordinates of the center of bending torsion (x_P, y_P) to be expanded in ϵ. The notation $x_P = x_P^0 + \epsilon\, x_P^1$ and $y_P = y_P^0 + \epsilon\, y_P^1$ is used. It can be determined that $(x_P^0, y_P^0) = (0, 0)$ and

$$x_{\mathrm{F}}^1 = -(1/\mathrm{I})\int_0^{2\pi}[\Phi_{0B}(a_o,\theta)\,a_o\,f_o'(\theta) - \Phi_{0B}(a_i,\theta)\,a_i\,f_i'(\theta)]d\theta \tag{3.20}$$

$$y_{\mathrm{F}}^1 = (1/\mathrm{I})\int_0^{2\pi}[\Phi_{0A}(a_o,\theta)\,a_o\,f_o'(\theta) - \Phi_{0A}(a_i,\theta)\,a_i\,f_i'(\theta)]d\theta$$

It follows that the twisting moment $\mathrm{M_F}$ is then

$$\mathrm{M_F} = \mathrm{M}_z + \epsilon(\mathrm{T}_x y_{\mathrm{F}}^1 - \mathrm{T}_y x_{\mathrm{F}}^1).$$

The twist $\hat{\theta}$ due to $\mathrm{M_F}$ also depends on J, which can be developed from equation (3.11) using the expansion $\mathrm{J} = \mathrm{J}_0 + \epsilon\mathrm{J}_1$. From the definition of J,

$$J = 2\int_0^{2\pi}\int_0^{a_i+\epsilon f_i(\theta)}(\alpha_{i0} + \epsilon\alpha_{i1})\,r\,dr d\theta \tag{3.21}$$
$$+ 2\int_0^{2\pi}\int_{a_i+\epsilon f_i(\theta)}^{\alpha_0+\epsilon f_o(\theta)}(\Theta_0 + \epsilon\Theta_1)\,r\,dr d\theta,$$

from which J_0 and J_1 can be obtained. The twist of the centroidial fiber is $\hat{\theta} = \hat{\theta}_0 + \epsilon\hat{\theta}_1$, and it can be shown that

$$\hat{\theta}_0 = \frac{\mathrm{M}_z}{\mathrm{GJ}_0}$$
$$\hat{\theta}_1 = \frac{\mathrm{T}_x y_{\mathrm{F}}^1 - \mathrm{T}_y x_{\mathrm{F}}^1}{\mathrm{GJ}_0} - \frac{\mathrm{M}_z \mathrm{J}_1}{\mathrm{GJ}_0^2}.$$

The constant C, proportional to the twist of the centroidial fiber, has the expansion $C = C_0 + \epsilon C_1$. From the definition of this constant, eqn (3.14), it follows

that

$$(3.22)\quad C = \frac{2}{\mathrm{J}_0 + \epsilon\,\mathrm{J}_1}\Bigg[(A_0+\epsilon A_1)\Bigg\{\int_0^{2\pi}\int_0^{a_i+\epsilon f_i(\theta)}(\alpha_{i0}+\epsilon\alpha_{i1})r\,\sin\theta\,r\,dr d\theta + \int_0^{2\pi}\int_{a_i+\epsilon f_i(\theta)}^{a_o+\epsilon f_o(\theta)}[\Theta_0+\epsilon\Theta_1]r\,\sin\theta\,r\,dr d\theta\Bigg\} - (B_0+\epsilon B_1)\Bigg\{\int_0^{2\pi}\int_0^{a_i+\epsilon f_i(\theta)}(\alpha_{i0}+\epsilon\alpha_{i1})r\,\cos\theta\,r\,dr d\theta + \int_0^{2\pi}\int_{a_i+\epsilon f_i(\theta)}^{a_o+\epsilon f_o(\theta)}[\Theta_0+\epsilon\Theta_1]r\,\cos\theta\,r\,dr d\theta\Bigg\}\Bigg],$$

from which C_0 and C_1 can be obtained. Note that A, B are given in terms of their corresponding expansions as well. Each of these parameters is explicitly defined and used in the derivation of the differential equations. From the notation (3.17) for the moments and products of inertia,

$$A_0 = \mathrm{T}_x/\mathrm{EI} \qquad B_0 = \mathrm{T}_y/\mathrm{EI}$$

$$A_1 = -(\mathrm{I}^1_{xy}\mathrm{T}_y + \mathrm{I}^1_{xx}\mathrm{T}_x)/\mathrm{EI}^2 \qquad B_1 = -(\mathrm{I}^1_{xy}\mathrm{T}_x + \mathrm{I}^1_{yy}\mathrm{T}_y)/\mathrm{EI}^2.$$

The shear stresses are then given in terms of the defined functions and parameters in accordance with eqn (3.4) and the corresponding pertubation expansions:

$$(3.23)\quad \tau_{xz} = \mathrm{E}\frac{\partial\Phi_0}{\partial x} + \mathrm{G}\left(\frac{\partial \mathrm{K}_0}{\partial y} + \hat{\theta}_0\frac{\partial\Theta_0}{\partial y}\right) + \epsilon\left[\mathrm{E}\frac{\partial\Phi_1}{\partial x} + \mathrm{G}\left(\frac{\partial \mathrm{K}_1}{\partial y} + \hat{\theta}_0\frac{\partial\Phi_1}{\partial y} + \hat{\theta}_1\frac{\partial\Theta_0}{\partial y}\right)\right]$$

$$\tau_{yz} = \mathrm{E}\frac{\partial\Phi_0}{\partial y} - \mathrm{G}\left(\frac{\partial \mathrm{K}_0}{\partial x} + \hat{\theta}_0\frac{\partial\Theta_0}{\partial x}\right) + \epsilon\left[\mathrm{E}\frac{\partial\Phi_1}{\partial y} - \mathrm{G}\left(\frac{\partial \mathrm{K}_1}{\partial x} + \hat{\theta}_0\frac{\partial\Phi_1}{\partial x} + \hat{\theta}_1\frac{\partial\Theta_0}{\partial x}\right)\right]$$

3.2. PERTUBATION ANALYSIS

Although the shear stresses have been derived, the goal of this model is to obtain the normal and tangential components of the shear stresses along the outer and inner surfaces of the bone. These components, τ_{NZ}, τ_{TZ}, respectively, are given in terms of τ_{xz}, τ_{yz} by

(3.25)
$$\tau_{\mathrm{NZ}} = \tau_{xz}\cos\phi + \tau_{yz}\sin\phi$$
$$\tau_{\mathrm{TZ}} = -\tau_{xz}\sin\phi + \tau_{yz}\cos\phi,$$

where ϕ is the angle that the outward pointing normal makes with the x-axis. Since ϕ differs from θ only to order ϵ, we define the quantity ζ according to

$$\epsilon\,\zeta = \theta - \phi.$$

Now $\epsilon\,\zeta$ is a small quantity, which allows the approximations $\cos(\epsilon\,\zeta) \approx 1 - (\epsilon\,\zeta)^2$ and $\sin(\epsilon\,\zeta) \approx \epsilon\,\zeta$. It then follows that

(3.26)
$$\begin{aligned}
\tau_{\mathrm{NZ}} = {} & \hat{\theta}_0\mathrm{G}\frac{1}{r}\frac{\partial\Theta_0}{\partial\theta} + \mathrm{E}\frac{\partial\Phi_0}{\partial r} + \mathrm{G}\frac{1}{r}\frac{\partial\mathrm{K}_0}{\partial\theta} \\
& + \epsilon\left\{\hat{\theta}_0\mathrm{G}\left(\frac{1}{r}\frac{\partial\Theta_1}{\partial\theta} + \zeta\,\frac{\partial\Theta_0}{\partial r}\right) + \hat{\theta}_1\mathrm{G}\frac{1}{r}\frac{\partial\Theta_0}{\partial\theta}\right. \\
& \qquad \left. + \mathrm{E}\left(\frac{\partial\Phi_1}{\partial r} - \zeta\frac{1}{r}\frac{\partial\Phi_0}{\partial\theta}\right) + \mathrm{G}\left(\frac{1}{r}\frac{\partial\mathrm{K}_1}{\partial\theta} + \zeta\frac{\partial\mathrm{K}_0}{\partial r}\right)\right\} \\
\tau_{\mathrm{TZ}} = {} & -\hat{\theta}_0\mathrm{G}\frac{\partial\Theta_0}{\partial r} + \mathrm{E}\frac{1}{r}\frac{\partial\Phi_0}{\partial\theta} - \mathrm{G}\frac{\partial\mathrm{K}_0}{\partial r} \\
& + \epsilon\left\{\hat{\theta}_0\mathrm{G}\left(-\frac{\partial\Theta_1}{\partial r} - \zeta\,\frac{1}{r}\frac{\partial\Theta_0}{\partial\theta}\right) - \hat{\theta}_1\mathrm{G}\frac{\partial\Theta_0}{\partial r}\right. \\
& \qquad \left. + \mathrm{E}\left(\frac{1}{r}\frac{\partial\Phi_1}{\partial\theta} - \zeta\frac{\partial\Phi_0}{\partial r}\right) + \mathrm{G}\left(-\frac{\partial\mathrm{K}_1}{\partial r} - \zeta\,\frac{1}{r}\frac{\partial\mathrm{K}_0}{\partial\theta}\right)\right\}
\end{aligned}$$

Evaluating these expressions on the inner and outer boundaries, $r = a_i$ and $r = a_o$, respectively, yields the desired results.

In summary, regarding the cross section of the bone as a perturbed circular annulus, all of the definitions can be rewritten in terms of an expansion in terms of ϵ. Then all of the corresponding parameters and equations can be derived as also having two parts, zero order and first order. Finally, the equations for the stresses can be developed in terms of these definitions and parameters.

The differential equations, boundary conditions, and circuit conditions for the expansions of Θ, Φ and K will now be expressed. After each pair of initial value problems there are brief notational and informative remarks. Then explicit forms for the expansions of J, $\hat{\theta}$ and C are expressed as derived from their corresponding definitions. Henceforth, it is assumed that the independent variables are the polar coordinates (r, θ), unless otherwise stated.

The equation for Θ_0 is

$$\nabla^2\Theta_0 = -2 \tag{3.27}$$

with boundary conditions

$$\Theta_0(a_o, \theta) = 0 \tag{3.28}$$

$$\Theta_0(a_i, \theta) = \alpha_{i0}$$

and circuit condition

$$-a_i \int_0^{2\pi} \frac{\partial\Theta_0(a_i, \theta)}{\partial r} d\theta = 2\pi a_i^2. \tag{3.29}$$

The equation for Θ_1 is

$$\nabla^2\Theta_1 = 0 \tag{3.30}$$

with boundary conditions

$$\Theta_1(a_o,\theta) = -f_o(\theta)\frac{\partial\Theta_0(a_i,\theta)}{\partial r} \tag{3.31}$$
$$\Theta_1(a_i,\theta) = \alpha_{i1} - f_i(\theta)\frac{\partial\Theta_0(a_i,\theta)}{\partial r}$$

and circuit condition

$$-a_i\int_0^{2\pi}\frac{\partial\Theta_1(a_i,\theta)}{\partial r}d\theta \tag{3.32}$$
$$= \int_0^{2\pi}\left\{f_i(\theta)\frac{\partial\Theta_0(a_i,\theta)}{\partial r} - \frac{f_i'(\theta)}{a_i}\frac{\partial\Theta_0(a_i,\theta)}{\partial\theta} + a_i f_i(\theta)\frac{\partial\Theta_0^2(ai,\theta)}{\partial r^2}\right\}d\theta.$$

For α_i, the expression $\alpha_i = \alpha_{i0} + \epsilon\,\alpha_{i1}$ is used. Note that the differential equations are defined on the annulus $a_i \le r \le a_o, 0 \le \theta \le 2\pi$. The boundary condition on c_0 was found by expanding

$$\Theta_0(a_o + \epsilon f_o(\theta),\theta) + \epsilon\Theta_1(a_o + \epsilon f_o(\theta),\theta) = 0$$

in an asymptotic series in ϵ. The boundary condition on c_i is derived in an analagous manner. The circuit condition is developed from an asymptotic expansion in ϵ of the gradient of Θ_0 and the normal derivative to curves c_o and c_i. Note that the area Ω_i is given exactly by πa_i^2, as reflected in the circuit condition for Θ_0.

The equation for Φ_0 is

$$\nabla^2\Phi_0 = -r(A_0\cos(\theta) + B_0\sin(\theta)) \tag{3.33}$$

with boundary conditions

$$\frac{\partial\Phi_0(a_o,\theta)}{\partial r} = 0, \quad \frac{\partial\Phi_0(a_i,\theta)}{\partial r} = 0. \tag{3.34}$$

The equation for Φ_1 is

$$\nabla^2\Phi_1 = -r(A_1\cos(\theta) + B_1\sin(\theta)) \tag{3.35}$$

with boundary conditions

$$\begin{aligned}\frac{\partial\Phi_1(a_o,\theta)}{\partial r} &= -f_o(\theta)\frac{\partial^2\Phi_0(a_o,\theta)}{\partial r^2} + \frac{f_o'(\theta)}{a_o^2}\frac{\partial\Phi_0(a_o,\theta)}{\partial\theta} \\ \frac{\partial\Phi_1(a_i,\theta)}{\partial r} &= -f_i(\theta)\frac{\partial^2\Phi_0(a_i,\theta)}{\partial r^2} + \frac{f_i'(\theta)}{a_i^2}\frac{\partial\Phi_0(a_i,\theta)}{\partial\theta}.\end{aligned} \tag{3.36}$$

For A and B, the expansions $A = A_0 + \epsilon A_1$, $B = B_0 + \epsilon B_1$ are used, where A_0, A_1, B_0, B_1 are defined in eqn (3.2.1). Again, the differential equations for Φ_0 and Φ_1 are defined in the annulus $a_i \le r \le a_o, 0 \le \theta \le 2\pi$. The boundary conditions were derived from the result in eqn (3.8).

The equation for K_0 is

$$\nabla^2 K_0 = 2\nu r(A_0 \sin(\theta) - B_0 \cos(\theta) - C_0) \tag{3.37}$$

with boundary conditions

$$K_0(a_o, \theta) = 0 \tag{3.38}$$

$$K_0(a_i, \theta) = \beta_{i0}$$

and circuit condition

$$-a_i \int_0^{2\pi} \frac{\partial K_0(a_i, \theta)}{\partial r} d\theta = 2\nu a_i^2 C_0. \tag{3.39}$$

The equation for K_1 is

$$\nabla^2 K_1 = 2\nu r(A_1 \sin(\theta) - B_1 \cos(\theta) - C_1) \tag{3.40}$$

with boundary conditions

$$K_1(a_o, \theta) = -f_o(\theta) \frac{\partial K_0(a_o, \theta)}{\partial r} \tag{3.41}$$

$$K_1(a_i, \theta) = \beta_{i1} - f_i(\theta) \frac{\partial K_0(a_i, \theta)}{\partial r}$$

and circuit condition

$$\begin{aligned} -a_i \int_0^{2\pi} \frac{\partial K_1(a_i, \theta)}{\partial r} d\theta &= 2\nu\pi a_i^2 (B_0 \hat{x}_i - A_0 \hat{y}_i + C_1) \\ &+ \int_0^{2\pi} \left\{ f_i(\theta) \frac{\partial K_0(a_i, \theta)}{\partial r} - \frac{f_i'(\theta)}{a_i} \frac{\partial K_0(a_i, \theta)}{\partial \theta} \right. \\ &\left. + a_i f_i(\theta) \frac{\partial^2 K_0(a_i, \theta)}{\partial r^2} \right\} d\theta. \end{aligned} \tag{3.42}$$

For β_i and C, the expansions $\beta_i = \beta_{i0} + \epsilon\beta_{i1}$, $C = C_0 + \epsilon C_1$ are used, where C_0, C_1 are derived from eqn (3.22). The boundary value problems for K_0, K_1 are defined

on the annulus $a_i \leq r \leq a_o, 0 \leq \theta \leq 2\pi$. The constant C, which is written in terms of its pertubation expansion, also depends on the geometry of the body. The circuit condition contains $\hat{x}_i$, $\hat{y}_i$; to emphasise the fact that the centroid is $O(\epsilon)$, its coordinates were written in the form $(\epsilon\,\hat{x}_i,\ \epsilon\,\hat{y}_i)$.

The parameters J_0, J_1 and the constants C_0, C_1 are determined from expanding each of their definitions (3.21), (3.22). To evaluate the integrations for these, the following transformation is used:

$$r = a_i + \epsilon f_i(\theta) + s\,[a_o + \epsilon f_o(\theta) - a_i - \epsilon f_i(\theta)]$$

After applying the transformation, the following expressions can be derived for J_0, J_1:

$$\text{(3.43)}\quad J_0 = 2\pi a_i^2 \alpha_{i0} + 2\int_0^{2\pi}\int_0^1 \Theta_0(a_i + s(a_0 - a_i), \theta)[a_i + s(a_0 - a_i)](a_o - a_i)\,ds\,d\theta$$

$$\begin{aligned}\text{(3.44)}\quad J_1 &= 2\pi a_i^2 \alpha_{i1} \\ &+ 2\int_0^{2\pi}\int_0^1 \Theta_0(a_i + s(a_0 - a_i), \theta)[a_i + s(a_0 - a_i)](f_o(\theta) - f_i(\theta))\,ds\,d\theta \\ &+ 2\int_0^{2\pi}\int_0^1 \Theta_0(a_i + s(a_0 - a_i), \theta)[f_i(\theta) + s\,(f_o(\theta) - f_i(\theta))][a_i + s(a_0 - a_i)](a_o - a_i)\,ds\,d\theta \\ &+ 2\int_0^{2\pi}\int_0^1 \frac{\partial}{\partial r}\Theta_0(a_i + s(a_0 - a_i), \theta)[f_i(\theta) + s(f_o(\theta) - f_i(\theta))][a_i + s(a_0 - a_i)](a_o - a_i)\,ds\,d\theta \\ &+ 2\int_0^{2\pi}\int_0^1 \Theta_1(a_i + s(a_0 - a_i), \theta)[a_i + s(a_0 - a_i)](a_o - a_i)\,ds\,d\theta\end{aligned}$$

Similarly the following expressoins can be derived for C_0, C_1:

$$\begin{aligned}\text{(3.45)}\quad C_0 = \frac{2}{J_0}\int_0^{2\pi}\int_0^1 &\Theta_0(a_i + s(a_0 - a_i), \theta)[a_i + s(a_0 - a_i)]^2 \\ &(a_o - a_i)(A_0 \sin\theta - B_0 \cos\theta)\,ds\,d\theta\end{aligned}$$

$$
\begin{aligned}
(3.46)\quad C_1 = \frac{2}{\mathrm{J}_0}\int_0^{2\pi}\int_0^1 \Big[(A_1 - \frac{A_1\mathrm{J}_1}{\mathrm{J}_0})\sin\theta - (B_1 - \frac{B_0\mathrm{J}_1}{\mathrm{J}_0}\cos\theta\Big] \\
[a_i + s(a_0 - a_i)]^2(a_o - a_i)\Theta_0(a_i + s(a_0 - a_i),\theta)dsd\theta \\
+ \frac{2}{\mathrm{J}_0}\alpha_{i0}a_i^2\int_0^{2\pi} f_i(\theta)(A_0\sin\theta - B_0\cos\theta)d\theta \\
+ \frac{2}{\mathrm{J}_0}\int_0^{2\pi}\int_0^1 (A_0\sin\theta - B_0\cos\theta)\Big\{\Big[[a_i + s(a_0 - a_i)]^2(f_o - f_i) \\
+ 2[a_i + s(a_0 - a_i)][f_i + s\,(f_o - f_i)](a_o - a_i)\Big]\Theta_0(a_i + s(a_0 - a_i),\theta) \\
+ [f_i + s(f_o - f_i)][a_i + s(a_0 - a_i)]^2(a_o - a_i)\frac{\partial}{\partial r}\Theta_0(a_i + s(a_0 - a_i),\theta) \\
+ (a_o - a_i)[a_i + s(a_0 - a_i)]^2\Theta_1(a_i + s(a_0 - a_i),\theta)\Big\}dsd\theta.
\end{aligned}
$$

3.2.2 Zero Order Solution

The zero order solution pertains to the annulus, which has an outer radius of a_o and an inner radius of a_i. The solution to the boundary value problems for Θ_0, Φ_0 and K_0 expressed in the previous section are straightforward, and the results are given here:

$$\Theta_0 = (a_o^2 - r^2)/2 \tag{3.47}$$

$$\Phi_0 = \frac{3}{8}(A_0 \cos\theta + B_0 \sin\theta)\left[(a_o^2 + a_i^2)r + \frac{a_o^2 a_i^2}{r} - \frac{r^3}{3}\right]$$

$$K_0 = \frac{\nu}{4}(B_0 \cos\theta - A_0 \sin\theta)\left[(a_o^2 + a_i^2)r - \frac{a_o^2 a_i^2}{r} - r^3\right]$$

By writing the differential operator ∇^2 in polar form, *ie.*

$$\nabla^2(\cdot) = \frac{\partial}{\partial r^2}(\cdot) + \frac{1}{r}\frac{\partial}{\partial r}(\cdot) + \frac{1}{r^2}\frac{\partial}{\partial \theta^2}(\cdot),$$

it is easy to verify that the zero order solutions solve the corresponding differential equations (3.27), (3.33) and (3.37). Note that Θ_0 is a function of r alone. Two results from this solution are, from eqn. (3.43), $J_0 = (\pi/2)(a_o^4 - a_i^4)$, and from eqn. (3.45), $C_0 = 0$.

The stresses in the circular annulus are

$$\sigma_{z0} = \frac{T_z}{\pi(a_o^2 - a_i^2)} - \frac{M_y}{I}\, r\cos\theta + \frac{M_x}{I}\, r\sin\theta \tag{3.48}$$

(3.49)

$$\tau^0_{\rm NZ} = \frac{3}{8}\,{\rm E}\,(A_0\cos\theta + B_0\sin\theta)\left[a_o^2 + a_i^2 - \frac{a_o^2 a_i^2}{r^2} - r^2\right]$$
$$+ \frac{\nu}{4}\,{\rm G}\,(A_0\sin\theta - B_0\cos\theta)\left[a_o^2 + a_i^2 - \frac{a_o^2 a_i^2}{r^2} - r^2\right]$$
$$\tau^0_{\rm TZ} = \frac{3}{8}\,{\rm E}\,(B_0\cos\theta - A_0\sin\theta)\left[a_o^2 + a_i^2 + \frac{a_o^2 a_i^2}{r^2} - \frac{r^2}{3}\right]$$
$$- \frac{\nu}{4}\,{\rm G}\,(B_0\cos\theta + A_0\sin\theta)\left[a_o^2 + a_i^2 - \frac{a_o^2 a_i^2}{r^2} - 3r^2\right] + {\rm G}\,\hat{\theta}_o\, r$$

Note that on the inner and outer edges of the annulus the normal stress $\tau_{\rm NZ}$ is zero, as it should be.

3.2.3 First Order Solution

The pertubed outer and inner boundaries of the bone are approximated by a finite Fourier series:

(3.50)
$$f_o(\theta) = \sum_{n=1}^{M}\left(a_{on}\cos n\theta + b_{on}\sin n\theta\right)$$
$$f_i(\theta) = \sum_{n=1}^{M}\left(a_{in}\cos n\theta + b_{in}\sin n\theta\right)$$

The origin of the coordinate system is assumed to be at the centroid of the cross section. Then the coefficients of this expansion must satisfy

(3.51)
$$a_o^2 a_{o1} - a_i^2 a_{i1} = 0$$
$$a_o^2 b_{o1} - a_i^2 b_{i1} = 0$$

The first order contributions to the moments of inertia are:

(3.52)
$${\rm I}^1_{xx} = -{\rm I}^1_{yy} = \frac{\pi}{2}(a_o^3 a_{o2} - a_i^3 a_{i2})$$
$${\rm I}^1_{xy} = \frac{\pi}{2}(a_o^3 b_{o2} - a_i^3 b_{i2})$$

Then K_{x1}, K_{y1} are determined from eqn (3.18). Thus σ_{z1} follows from eqn (3.19). The moments of inertia also determine the parameters A_1, B_1; *ie.*

(3.53)
$$A_1 = -8[\mathrm{T}_y(a_o^3 b_{o2} - a_i^3 b_{i2}) + \mathrm{T}_x(a_o^3 a_{o2} - a_i^3 a_{i2})]/\mathrm{E}\,\pi(a_o^4 - a_i^4)^2.$$
$$B_1 = -8[\mathrm{T}_x(a_o^3 b_{o2} - a_i^3 b_{i2}) - \mathrm{T}_x(a_o^3 a_{o2} - a_i^3 a_{i2})]/\mathrm{E}\,\pi(a_o^4 - a_i^4)^2.$$

Substituting the zero order solution and the Fourier series expansion for f_o, f_i into the boundary value problem for Θ_1 gives the following boundary conditions:

(3.54)
$$\Theta_1(a_o, \theta) = a_o \sum_{n=1}^{M} (a_{on} \cos n\theta + b_{on} \sin n\theta)$$
$$\Theta_1(a_i, \theta) = a_i \sum_{n=1}^{M} (a_{in} \cos n\theta + b_{in} \sin n\theta)$$

With these, the circuit condition simplifies to

(3.55)
$$\int_0^{2\pi} \frac{\partial \Theta_1(a_i, \theta)}{\partial r} d\theta = 0.$$

For the boundary value problem for Φ_1, substituting our previous results for Φ_0 into the boundary conditions gives

$$\frac{\partial \Phi_1(a_o, \theta)}{\partial r} = \left[\frac{3(a_o^2 - a_i^2)}{4a_o}\right](A_0 \cos\theta + B_0 \sin\theta)\, f_o(\theta)$$
$$+ \frac{1}{4a_o}(a_o^2 + 3a_i^2)(-A_0 \sin\theta + B_0 \cos\theta)\, f_o'(\theta)$$
$$\frac{\partial \Phi_1(a_i, \theta)}{\partial r} = \left[\frac{3(a_i^2 - a_o^2)}{4a_i}\right](A_0 \cos\theta + B_0 \sin\theta)\, f_i(\theta)$$
$$+ \frac{1}{4a_i}(a_i^2 + 3a_o^2)(-A_0 \sin\theta + B_0 \cos\theta)\, f_i'(\theta)$$

After using the finite Fourier series, these equations can be simplified further by

using the following triginometric identities:

$$2\sin n\theta\cos\theta = \sin(n+1)\theta + \sin(n-1)\theta$$

$$2\cos n\theta\sin\theta = \sin(n+1)\theta - \sin(n-1)\theta$$

$$2\cos n\theta\cos\theta = \cos(n+1)\theta + \cos(n-1)\theta$$

$$2\sin n\theta\sin\theta = -\cos(n+1)\theta + \cos(n-1)\theta$$

Thus it can be shown that the boundary conditions for the boundary value problem involving Φ_1 can be written in the following compact manner:

(3.56)
$$\frac{\partial\Phi_1(a_o,\theta)}{\partial r} = l_{o0} + \sum_{n=1}^{M+1}(k_{on}\sin n\theta + l_{on}\cos n\theta)$$
$$\frac{\partial\Phi_1(a_o,\theta)}{\partial r} = l_{i0} + \sum_{n=1}^{M+1}(k_{in}\sin n\theta + l_{in}\cos n\theta),$$

where

(3.57)
$$l_{o0} = \frac{a_o}{2}(A_0a_{o1} + B_0b_{o1})$$
$$k_{on} = \left[\frac{3(a_o^2 - a_i^2)}{8a_o}\right]\left[A_0\left(b_{o(n-1)} + b_{o(n+1)}\right) + B_0\left(a_{o(n-1)} - a_{o(n+1)}\right)\right]$$
$$+ \left[\frac{a_o^2 + 3a_i^2}{8a_o}\right]\left[(n+1)\left(A_0b_{o(n+1)} - B_0a_{o(n+1)}\right)\right.$$
$$\left. - (n+1)\left(A_0b_{o(n-1)} + B_0a_{o(n-1)}\right)\right]$$

$$l_{on} = \left[\frac{3(a_o^2 - a_i^2)}{8a_o}\right]\left[A_0\left(a_{o(n-1)} + a_{o(n+1)}\right) + B_0\left(b_{o(n+1)} - b_{o(n-1)}\right)\right]$$
$$+ \left[\frac{a_o^2 + 3a_i^2}{8a_o}\right]\left[(n+1)\left(B_0b_{o(n+1)} - A_0a_{o(n+1)}\right)\right.$$
$$\left. - (n+1)\left(B_0b_{o(n-1)} + A_0a_{o(n-1)}\right)\right].$$

Analagous expressions define l_{i0}, k_{in} and l_{in}, with a_o, a_{on}, b_{on} replaced by a_i, a_{in}, b_{in}, respectively, and a_i replaced by a_o.

The boundary conditions for the boundary value problem to determine K_1 can also be explicitly derived. After substituting in the results for $f_o(\theta)$, $f_i(\theta)$, and $K_0(a_o, \theta)$, it can be readily shown that

$$K_1(a_o,\theta) = \frac{\nu}{2}(a_o^2 - a_i^2)\sum_{n=1}^{M}\Big[B_0\, a_{on}\cos\theta\cos n\theta + B_0\, b_{on}\cos\theta\sin n\theta - A_0\, a_{on}\sin\theta\cos n\theta - A_0\, b_{on}\sin\theta\sin n\theta\Big]$$

$$K_1(a_i,\theta) = \beta_{i1} - \frac{\nu}{2}(a_o^2 - a_i^2)\sum_{n=1}^{M}\Big[B_0\, a_{in}\cos\theta\cos n\theta + B_0\, b_{in}\cos\theta\sin n\theta - A_0\, a_{in}\sin\theta\cos n\theta - A_0\, b_{in}\sin\theta\sin n\theta\Big]$$

After applying trigonometric identities, it can be verified that the boundary conditions for the boundary value problem for K_1 can be written in the following compact form.

(3.60)

$$K_1(a_o,\theta) = \frac{\nu}{4}(a_o^2 - a_i^2)\Big[p_{o0} + \sum_{n=1}^{M+1} p_{on}\cos n\theta + q_{on}\sin n\theta\Big]$$

$$K_1(a_i,\theta) = \beta_{i1} - \frac{\nu}{4}(a_o^2 - a_i^2)\Big[p_{i0} + \sum_{n=1}^{M+1} p_{in}\cos n\theta + q_{in}\sin n\theta\Big],$$

where

(3.61)

$$p_{o0} = B_0 a_{o1} - A_0 b_{o1}$$

$$p_{on} = A_0\Big(b_{o(n-1)} - b_{o(n+1)}\Big) + B_0\Big(a_{o(n+1)} + a_{o(n-1)}\Big)$$

$$q_{on} = A_0\Big(a_{o(n+1)} - a_{o(n-1)}\Big) + B_0\Big(b_{o(n+1)} + b_{o(n-1)}\Big)$$

with analogous expressions for p_{i0}, p_{in}, q_{in} in which a_{on}, b_{on} are replaced by a_{in}, b_{in} respectively.

The circuit condition for K_1 follows from eqn (3.42). To help simplify this equation, the following two useful facts are used:

$$B_0\hat{x}_i - A_0\hat{y}_i = p_{i0}.$$

$$\int_0^{2\pi} f_i(\theta)\left[a_i\frac{\partial^2}{\partial r^2}\mathrm{K}_0(a_i,\theta) + \frac{\partial}{\partial r}\mathrm{K}_0(a_i,\theta)\right]d\theta = -2a_i^2\nu\,\pi\,p_{i0}.$$

The first fact comes from the definitions of $\hat{x}_i$, $\hat{y}_i$. The second fact can easily be verified. Using these to simplify the expression yields

$$\int_0^{2\pi}\frac{\partial \mathrm{K}_1(a_i,\theta)}{\partial r}d\theta = -\frac{1}{a_i}\left[2\nu\,\pi\,a_i^2C_1 - \int_0^{2\pi}\frac{f_i'(\theta)}{a_i}\frac{\partial \mathrm{K}_0(a_i,\theta)}{\partial\theta}d\theta\right].$$

The integral with respect to θ on the right hand side of this equation is equal to zero, so the circuit condition for K_1 is

$$\int_0^{2\pi}\frac{\partial \mathrm{K}_1(a_i,\theta)}{\partial r}d\theta = -2\nu\,\pi\,a_i\,C_1. \tag{3.62}$$

The boundary value problem for Θ_1 comes from eqn (3.30), with simplified boundary conditions (3.54), and circuit condition (3.55), and it is solved using standard techniques. It is found that $\alpha_{i1} = 0$, and

$$\Theta_1 = \sum_{n=1}^{M}\left[\frac{1}{a_o^{2n} - a_i^{2n}}\right]\Big\{(e_n\sin n\theta + f_n\cos n\theta)\,r^n + (a_o\,a_i)^{n+1}(g_n\sin n\theta + h_n\cos n\theta)\,r^{-n}\Big\} \tag{3.63}$$

where

(3.64)
$$e_n = a_o^{n+1} b_{on} - a_i^{n+1} b_{in}$$
$$f_n = a_o^{n+1} a_{on} - a_i^{n+1} a_{in}$$
$$g_n = a_o^{n-1} b_{in} - a_i^{n-1} b_{on}$$
$$h_n = a_o^{n-1} a_{in} - a_i^{n-1} a_{on}.$$

The boundary value problem for Φ_1 comes from eqn (3.35) with the boundary conditions (3.56), and its solution is found through standard techniques. The result is

(3.65)
$$\Phi_1 = a_o l_{o0} \ln r + \frac{3}{8}\left(B_1 \sin\theta + A_1 \cos\theta\right)\left[\left(a_i^2 - a_o^2\right) r + \frac{a_i^2 a_o^2}{r} - \frac{r^3}{3}\right] + \sum_{n=1}^{M+1}\left[\frac{1}{n(a_o^{2n} - a_i^{2n})}\right]\left\{\left(U_n \sin n\theta + V_n \cos n\theta\right) r^n + \left(a_o\, a_i\right)^{n+1}\left(M_n \sin n\theta + N_n \cos n\theta\right) r^{-n}\right\}$$

where

(3.66)
$$U_n = a_o^{n+1} k_{on} - a_i^{n+1} k_{in}$$
$$V_n = a_o^{n+1} l_{on} - a_i^{n+1} l_{in}$$
$$M_n = a_o^{n-1} k_{in} - a_i^{n-1} k_{on}$$
$$N_n = a_o^{n-1} l_{in} - a_i^{n-1} l_{on}.$$

The boundary value problem for K_1 comes from eqn (3.40), with simplified

boundary conditions (3.60), and circuit condition (3.62), and it is solved using standard techniques. It is found that

$$
\begin{aligned}
(3.67)\quad \mathrm{K}_1 = \frac{\nu}{4}(B_0\cos\theta - A_0\sin\theta)\left[(a_o^2+a_i^2)\,r - \frac{a_o^2a_i^2}{r} - r^3\right] \\
+ \frac{\nu C_1}{2}\left[\frac{a_o^2\ln a_i - a_i^2\ln a_o}{\ln\frac{a_i}{a_o}} - \frac{(a_o^2-a_i^2)}{\ln\frac{a_i}{a_o}} - r^2\right] \\
+ \beta_{i1}\ln\left(\frac{r}{a_o}\right)\Big/\ln\left(\frac{a_i}{a_o}\right) \\
+ \left[\frac{\nu(a_o^2-a_i^2)}{4\ln\frac{a_i}{a_o}}\right]\left[p_{o0}\ln\frac{a_i}{r} + p_{i0}\ln\frac{a_o}{r}\right] \\
+ \left[\frac{\nu(a_o^2-a_i^2)}{4}\right]\sum_{n=1}^{M+1}\left[\frac{1}{a_o^{2n}-a_i^{2n}}\right]\Big\{(P_n\sin n\theta + Q_n\cos n\theta)\,r^n \\
+ (a_o\,a_i)^n(R_n\sin n\theta + S_n\cos n\theta)\,r^{-n}\Big\}
\end{aligned}
$$

and

$$
(3.68)\qquad \beta_{i1} = \frac{\nu}{4}(a_o^2-a_i^2)[p_{o0}+p_{i0}+2C_1]
$$

where

$$
\begin{aligned}
(3.69)\qquad P_n &= a_o^n p_{on} + a_i^n p_{in} \\
Q_n &= a_o^n q_{on} + a_i^n q_{in} \\
R_n &= a_o^n p_{in} + a_i^n p_{on} \\
S_n &= a_o^n q_{in} + a_i^n q_{on}.
\end{aligned}
$$

To determine the value of the parameter J_1, first note that Θ_0 does not contain θ. Then the variables r, θ can be separated in every integral of the eqn (3.44). Upon integration with respect to θ, one can show that every term is zero. Therefore $\mathrm{J}_1 = 0$.

On term by term examination of eqn (3.46) for C_1, one finds that the first term is seperable in the independent variables s, θ, and so this term is zero. To make the other terms more manageable, let $u = a_i + s(a_o - a_i)$; also, let G represent the last part of the last term in the equation for C_1, *ie.*

$$G = \frac{2}{\mathrm{J}_0}\int_0^{2\pi}\int_{a_i}^{a_o}(A_0\sin\theta - B_0\cos\theta)\,u^2\Theta_1(u,\theta)\,dr d\theta.$$

Since Θ_0 is a function of u alone, one can separate the variables u, θ in the remaining terms, and integrate first with respect to θ. Noting that $\int_0^{2\pi} f_o(\theta)(A_0\sin\theta - B_0\cos\theta)d\theta = \pi(B_0 a_{o1} - A_0 b_{o1}) = \pi p_{o0}$., $\int_0^{2\pi} f_i(\theta)(A_0\sin\theta - B_0\cos\theta)d\theta = \pi(B_0 a_{i1} - A_0 b_{i1}) = \pi p_{i0}$, it can be shown that

$$\begin{aligned} C_1 = \frac{2}{\mathrm{J}_0}\alpha_{i0}\,a_i^2\,\pi p_{i0} &+ \frac{2}{\mathrm{J}_0}(\pi p_{o0} - \pi p_{i0})\int_{a_i}^{a_o}\frac{u^2\Theta_0}{a_o - a_i}du \\ &+ \frac{2}{\mathrm{J}_0}\pi p_{i0}\int_{a_i}^{a_o}\left(2u\Theta_0 + u^2\frac{d}{du}\Theta_0\right)du \\ &+ \frac{2}{\mathrm{J}_0}(\pi p_{o0} - \pi p_{i0})\int_{a_i}^{a_o}\frac{u - a_i}{a_o - a_i}\left(2u\Theta_0 + u^2\frac{d}{du}\Theta_0\right)du + G, \end{aligned}$$

$$\begin{aligned} = \frac{2}{\mathrm{J}_0}\alpha_{i0}\,a_i^2\,\pi p_{i0} &+ \frac{2\pi}{\mathrm{J}_0}\left(\frac{p_{o0} - p_{i0}}{a_o - a_i}\right)\int_{a_i}^{a_o}\left(3u^2\,\Theta_0 + u^3\frac{d}{du}\Theta_0\right)du \\ &+ \frac{2\pi}{\mathrm{J}_0}\left[p_{i0} - a_i\left(\frac{p_{o0} - p_{i0}}{a_o - a_i}\right)\right]\int_{a_i}^{a_o}\left(2u\,\Theta_0 + u^2\frac{d}{du}\Theta_0\right)du + G. \end{aligned}$$

Evaluating the two integrals, it follows that $C_1 = G$. After integration and collecting of like terms, one obtains:

$$C_1 = \frac{\pi}{2\mathrm{J}_0}(a_o^2 - a_i^2)\Big[A_0(a_o^2 b_{o1} + a_i^2 b_{i1}) - B_0(a_o^2 a_{o1} + a_i^2 a_{i1})\Big]. \tag{3.72}$$

Chapter 4

Integration of Software & Results

The next step is to make the program that calculates stresses in the cross section compatible with the program that generates the Fourier series representation of the boundaries. It was found that the best way to combine the two was to develop a program to create disk data files that the program for the stresses could read and analyze. The filing structure for which the data and results for an entire bone would be stored was developed, so that they could be found and retrieved with ease.

From an enlarged photograph of one cross section, Phillipy [2] calculated its centroid, then using this as the origin he picked out 36 points, one at every ten degrees along each edge. He used the software to calculate the Fourier series coefficients. The centroid for the shape represented by the Fourier series was then calculated and, using this as the new origin, the process was continued until the origin selected and calculated converged to the same point. The same cross sectional slice was used in the present analysis with the camera and the program to produce coefficients for the Fourier series for each boundary as well and to automate the iteration. The resulting coefficients using Phillipy's method were very similiar to the ones from the

automated program. Thus the software was shown to produce accurate results. This software was then used to predict the stresses for an entire bone. The results were presented as graphs for each cross section, so that the stresses and their relation to the boundaries could be better understood. An outline of these results is given here.

In the actual bone which was used, the first cross section was given the global coordinate $z = 0$ cm; to account for the joint, cross section number 7 at $z = 1.478$ cm was considered to be where the bone is anchored as a cantelevered beam. The 30^{th} cross sectional slice was considered to be where the force is applied, as shown in figure 4.1. In order to calculate M_x and M_y, the distance from any cross section to cross section number 30 is needed.

For each cross section of the bone, 13 graphs were constructed. Each graph is given in polar coordinates. The first graph is a comparison of the actual boundaries and their corresponding Fourier series representation. As shown in figure 4.2, the actual points on the outer boundary and inner boundary are marked by discrete symbols, while the Fourier series representation of each boundary is shown by a continuous line.

The next set of four graphs,figures 4.3, 4.4, 4.5, 4.6, show the resulting zero and first order stresses, which were calculated using the mathematical model with a unit force applied in one direction, $T_x = 0$, $T_y = 1$, $T_z = 0$. Another set of graphs, included in the appendix, shows the results using a unit force applied to the direction $T_x = 1$, T_y=0, T_z=0. The graphs for two cross sections are included in the appendix, and the graphs of stresses for cross section number 21 with an applied unit force in the y-direction is used as an example to explain each different type of graph.

The tangential component of the plane stresses for the outer and inner boundaries of the bone comprise two of the four stress graphs. Each graph shows the magnitude of stress as a function of the angle in degrees, which marks the place along the particular boundary. The angle $\theta = 0$ corresponds to the positive x axis. The zero order stresses and the zero plus first order stresses are contrasted on the same graph. The tangential component of the plane stress τ_{TZ} is shown for each boundary; see figures 4.3, 4.4. The normal component of the plane stress τ_{NZ} is identically zero for the annulus, but small nonzero values are obtained for the first order solution, which reflect magnitudes of the errors introduced by the pertubation analysis.

The next two stress graphs, shown in figures 4.5, 4.6, are the normal stresses σ_z for the the outer and inner boundaries. Again, the magnitude of the stress is shown as a function of the angle along the boundary.

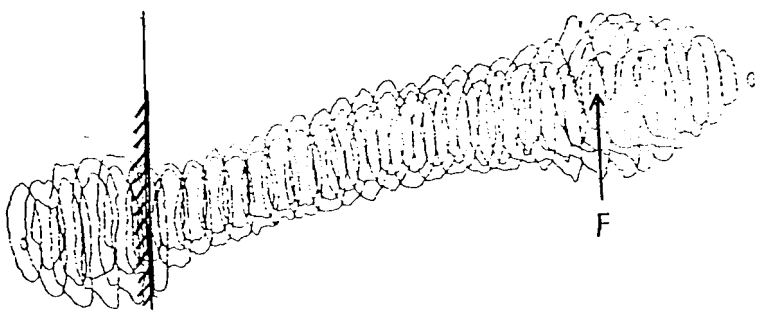

Figure 4.1: Static model of bone.

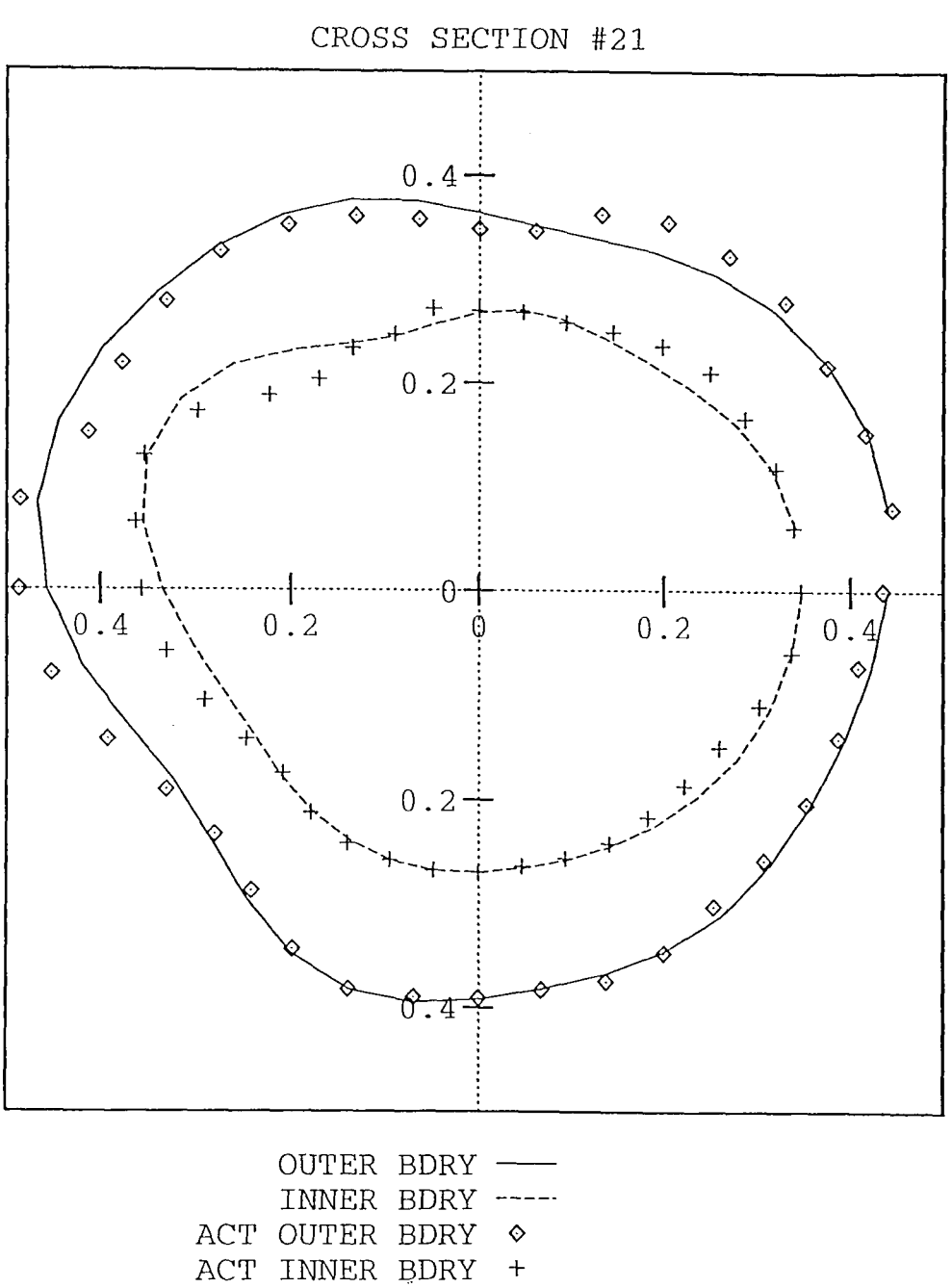

Figure 4.2: Boundaries of cross section.

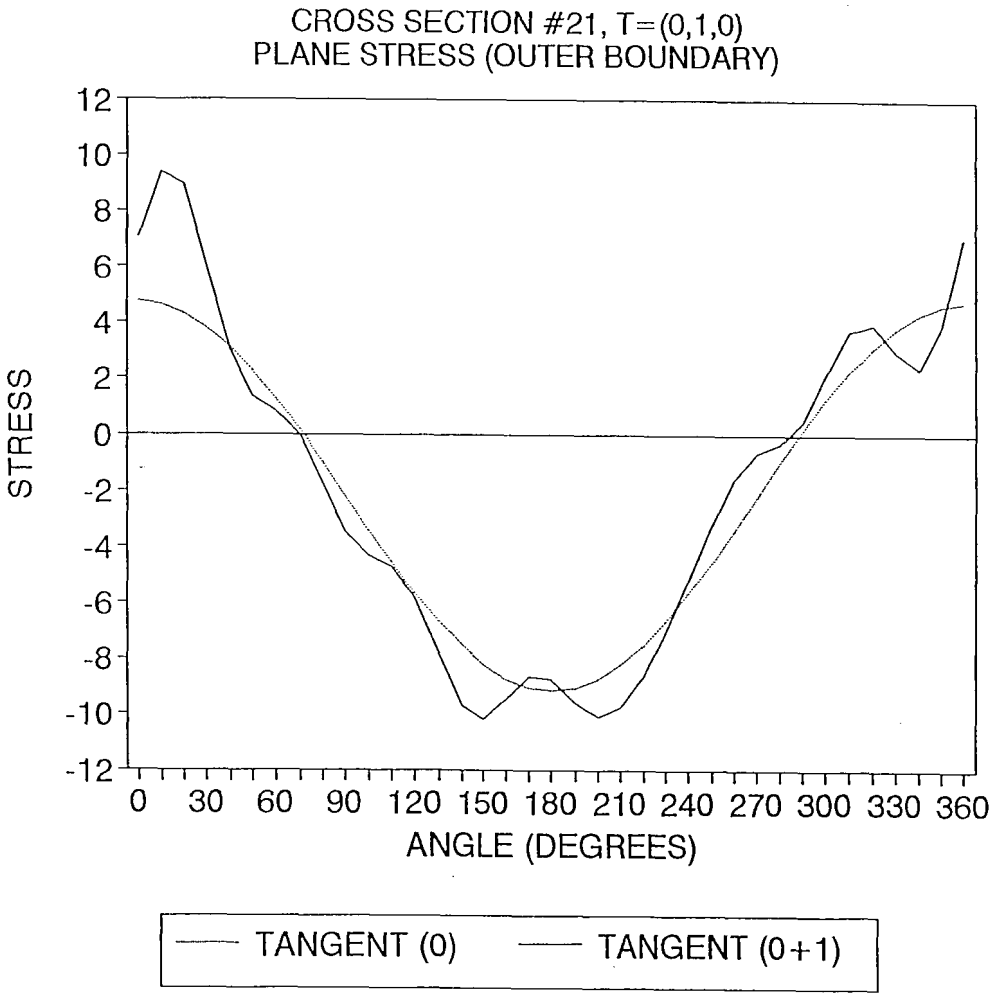

Figure 4.3: Tangential component of plane stress on outer boundary.

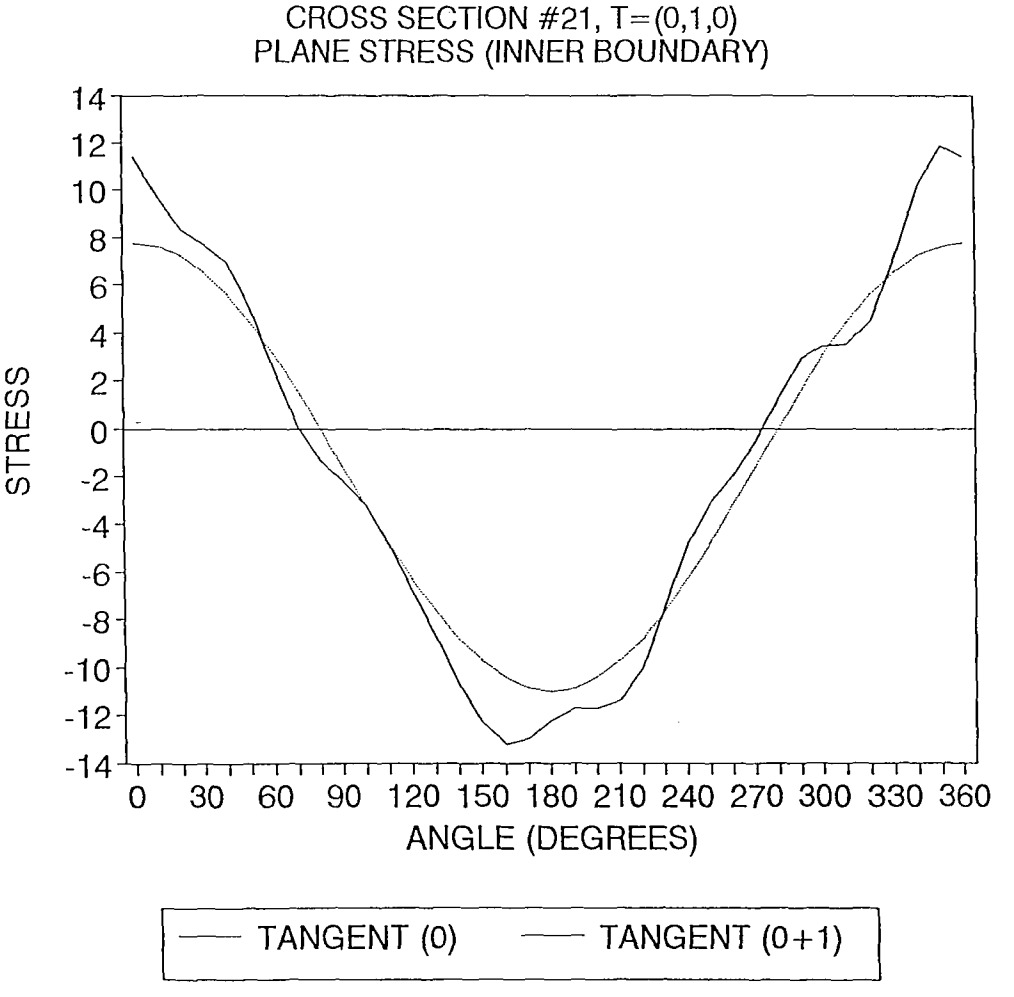

Figure 4.4: Tangential component of plane stress on inner boundary.

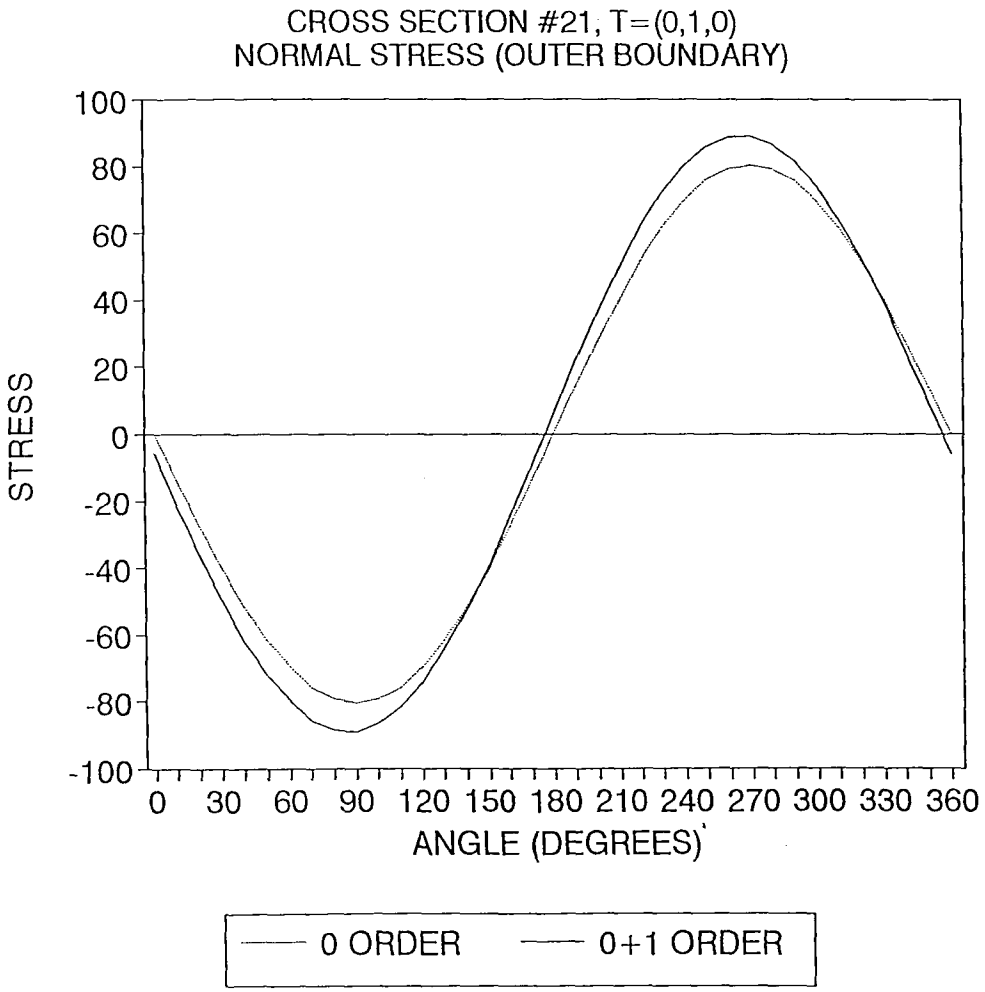

Figure 4.5: Normal stress σ_z on outer boundary.

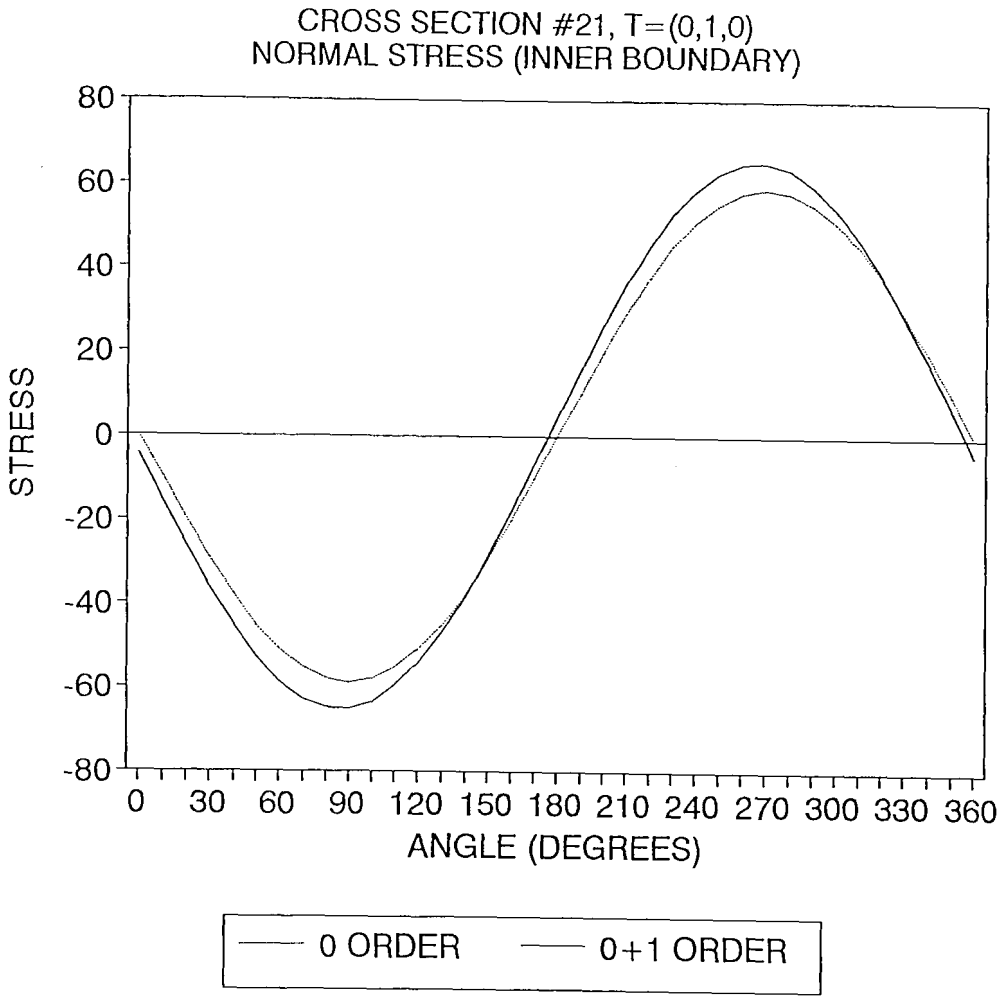

Figure 4.6: Normal stress σ_z on inner boundary.

Chapter 5

Conclusions

The orientation of the foot is assumed to be such that the metatarsals act as cantalevered beams. This study focuses on the stresses created within the fifth metatarsal under the influence of a force applied at one point along the bone. First, the bone is sliced into many cross sections. Specialized computer software is used to accurately and efficiently measure the boundaries of each cross section and compute the corresponding stresses along each boundary. The software uses results from the biomechanical analysis, which applies beam theory plus pertubation analysis to the bone.

In each cross section, the initial applied force is assumed to be one unit force component in one direction. The resulting data can then be combined to study the application of any general force applied at the same point as the initial force. If there is more than each force acting on the bone, the resultant force and moment applied at one point can be combined using superposition. Then for each cross section more general results can easily be obtained.

Altough clinical tests can be used to study the Jone's fracture, until now there

has not been a mathematical model developed to study the related types of stresses on the bone. The next step in the investigation for the Jone's fracture would be to use the results from the model to determine the necessary force at the approximate point of application that would cause the appropriate stresses. The mathematical model should reflect these stresses and be used to predict where along the bone the fracture would eventually occur.

To continue this study of the fifth metatarsal, the model can be used to analyze the stresses in a large sample of bones for a comprehensive statistical study. Even with the newly created software for this project, the study of this many bones with approximately 30 cross sections per bone would take a considerable amount of time. It is felt that ten bones, yeilding about 300 cross sections, could be used for a statistical analysis.

In order to analyze a fifth metatarsal in a patient, instead of a cadaver, CAT scanning can be used. Data on the boundaries of the bone collected from this process can be made into a useable form for the project software. Then this data can be applied to the same mechanical analysis to make a prediction as to whether or not this patient is at risk of getting the Jone's fracture.

Bibliography

[1] Salathé, Jr. E.P., Arangio, G.A., Salathé, E.P., "A Biomechanical Model of the Foot", *Journal Biomechanics*, 19, pp. 989-1001, (1986).

[2] Phillipy, D.C., "A Mathematical Analysis of a Biomechaminacal Model of the Foot", Phd. Thesis (Applied Mathematics), Lehigh University, (1991).

[3] de Veubeke, B.M.F., A Course in Elasticity, Springer-Verlag, New York, Heidelberg, Berlin, (1979).

Appendix A

Experimental Data

This appendix contains the results for three cross sections, numbers 20, 21 and 22. The graphs for numbers 20 and 22 are complete, while just the final set of results for cross section number 21, which has been used as example throughout this thesis, is included here. For description of the meaning of each graph, see Chapter 4.

CROSS SECTION #20

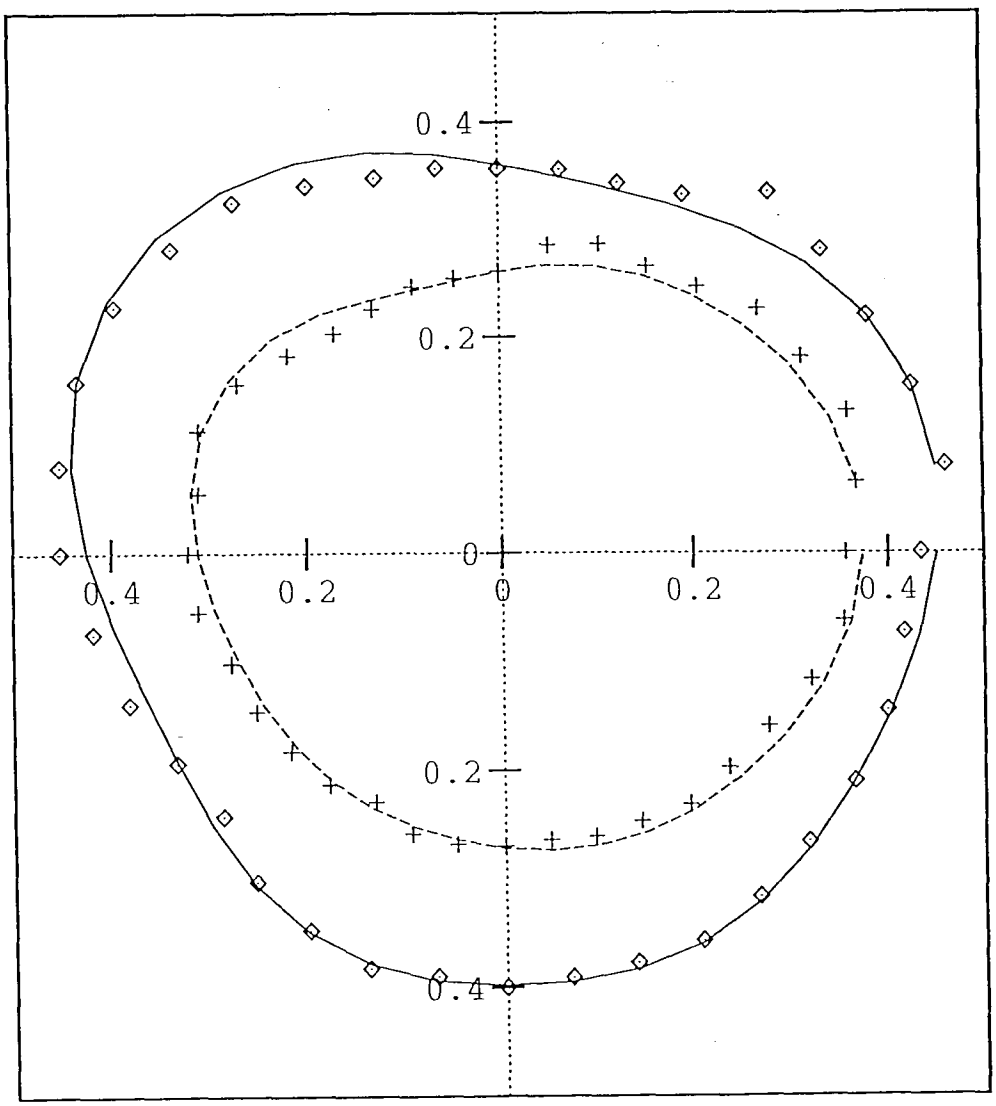

OUTER BDRY ——
INNER BDRY - - - -
ACT OUTER BDRY ◇
ACT INNER BDRY +

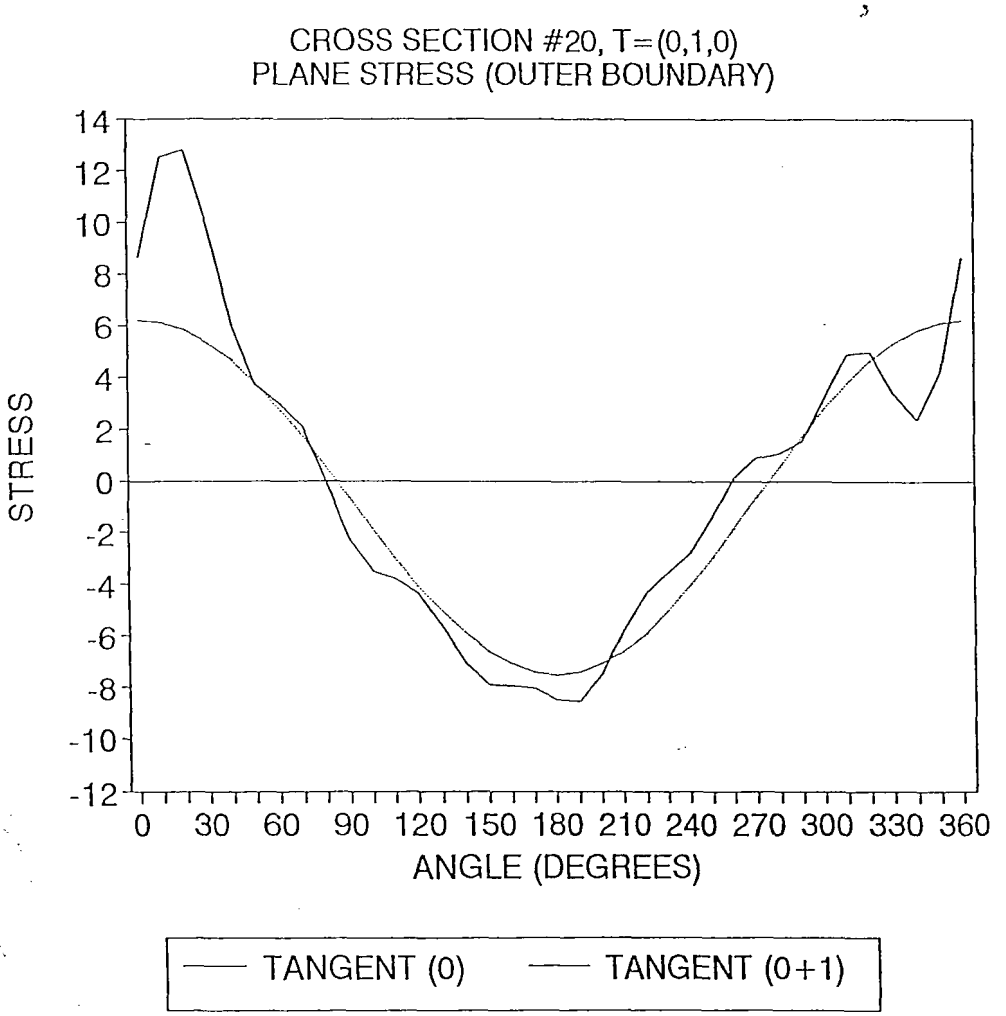
CROSS SECTION #20, T=(0,1,0)
PLANE STRESS (OUTER BOUNDARY)
STRESS
14
12
10
8
6
4
2
0
-2
-4
-6
-8
-10
-12
0 30 60 90 120 150 180 210 240 270 300 330 360
ANGLE (DEGREES)
TANGENT (0)
TANGENT (0+1)

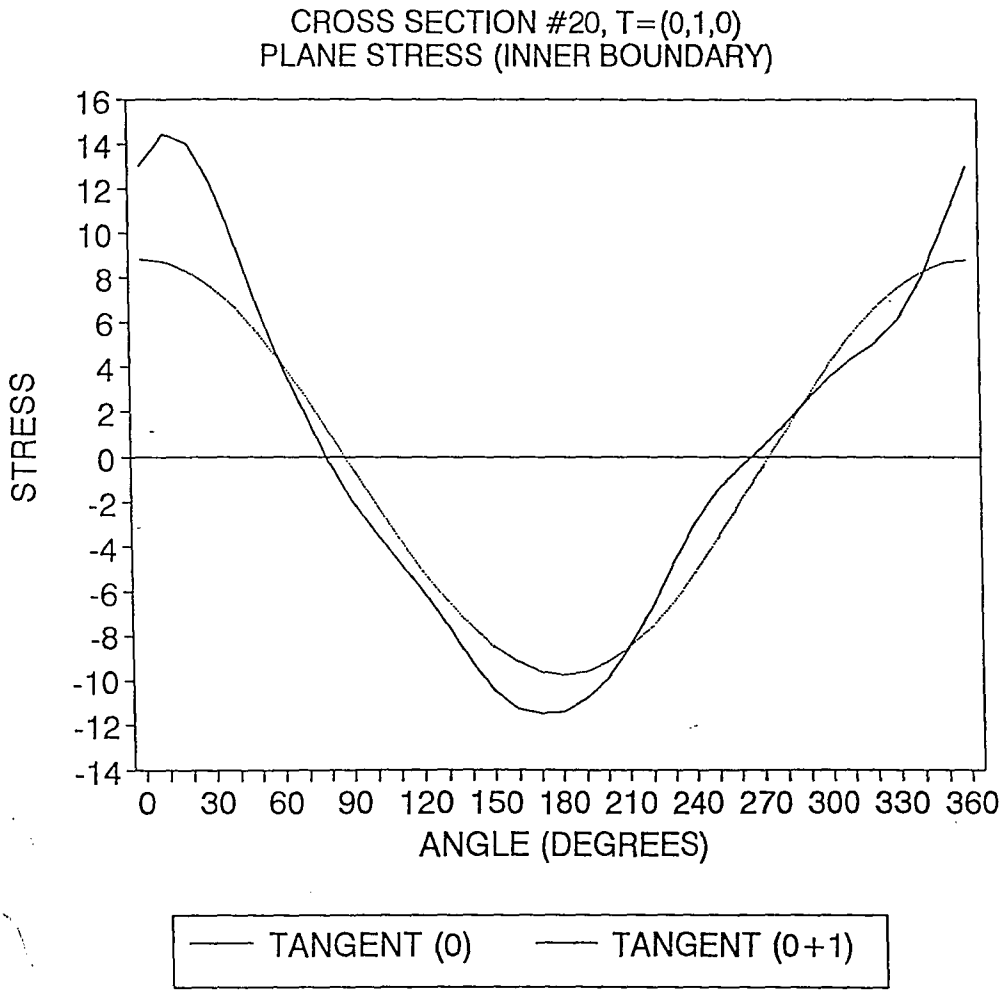
CROSS SECTION #20, T=(0,1,0)
PLANE STRESS (INNER BOUNDARY)
STRESS
16
14
12
10
8
6
4
2
0
-2
-4
-6
-8
-10
-12
-14
0 30 60 90 120 150 180 210 240 270 300 330 360
ANGLE (DEGREES)
TANGENT (0)
TANGENT (0+1)

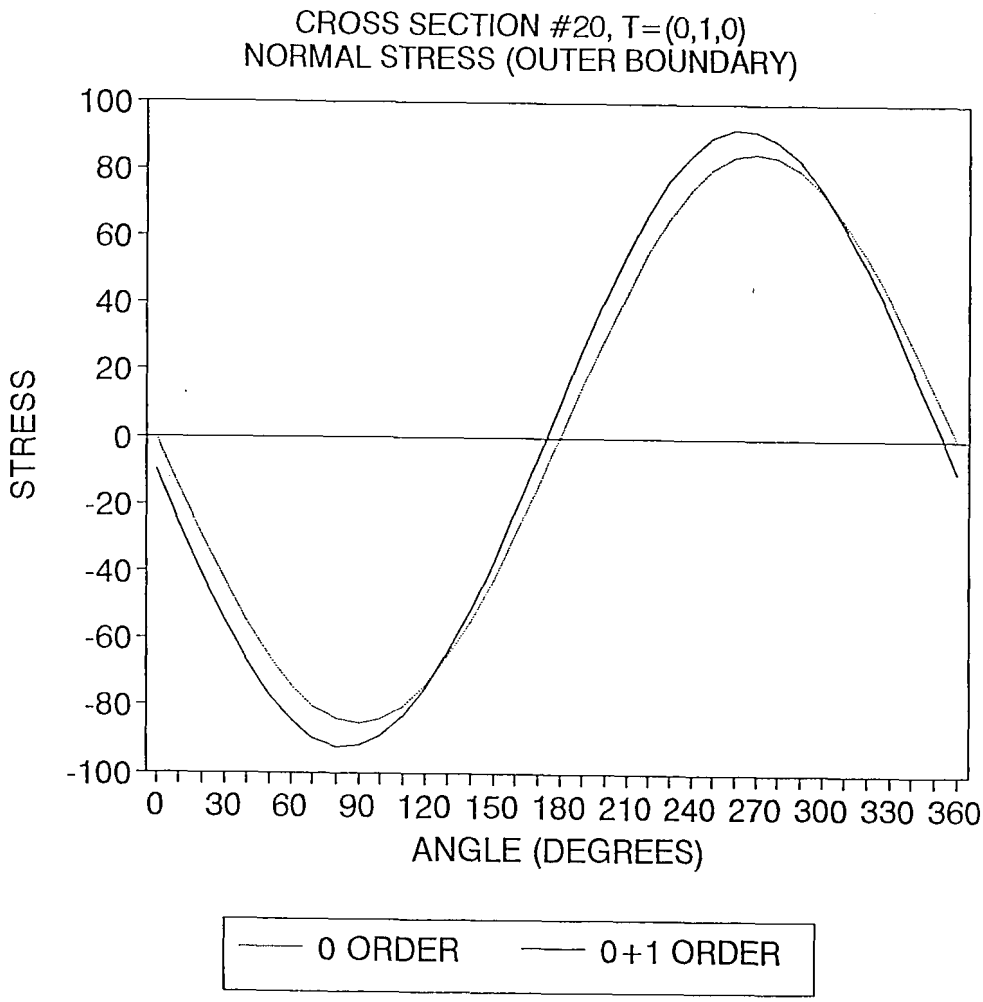
CROSS SECTION #20, T=(0,1,0)
NORMAL STRESS (OUTER BOUNDARY)
STRESS
100
80
60
40
20
0
-20
-40
-60
-80
-100
0 30 60 90 120 150 180 210 240 270 300 330 360
ANGLE (DEGREES)
0 ORDER
0+1 ORDER

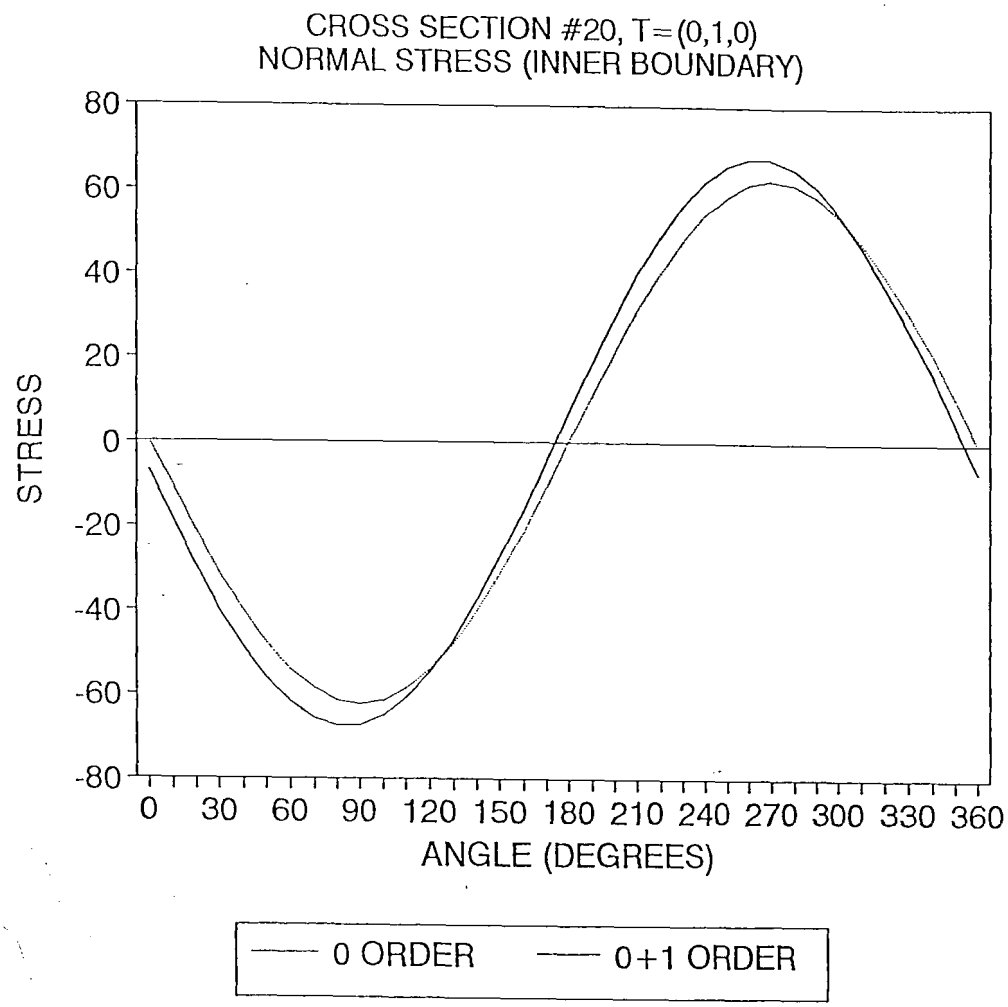
CROSS SECTION #20, T=(0,1,0)
NORMAL STRESS (INNER BOUNDARY)
STRESS
80
60
40
20
0
-20
-40
-60
-80
0 30 60 90 120 150 180 210 240 270 300 330 360
ANGLE (DEGREES)
0 ORDER
0+1 ORDER

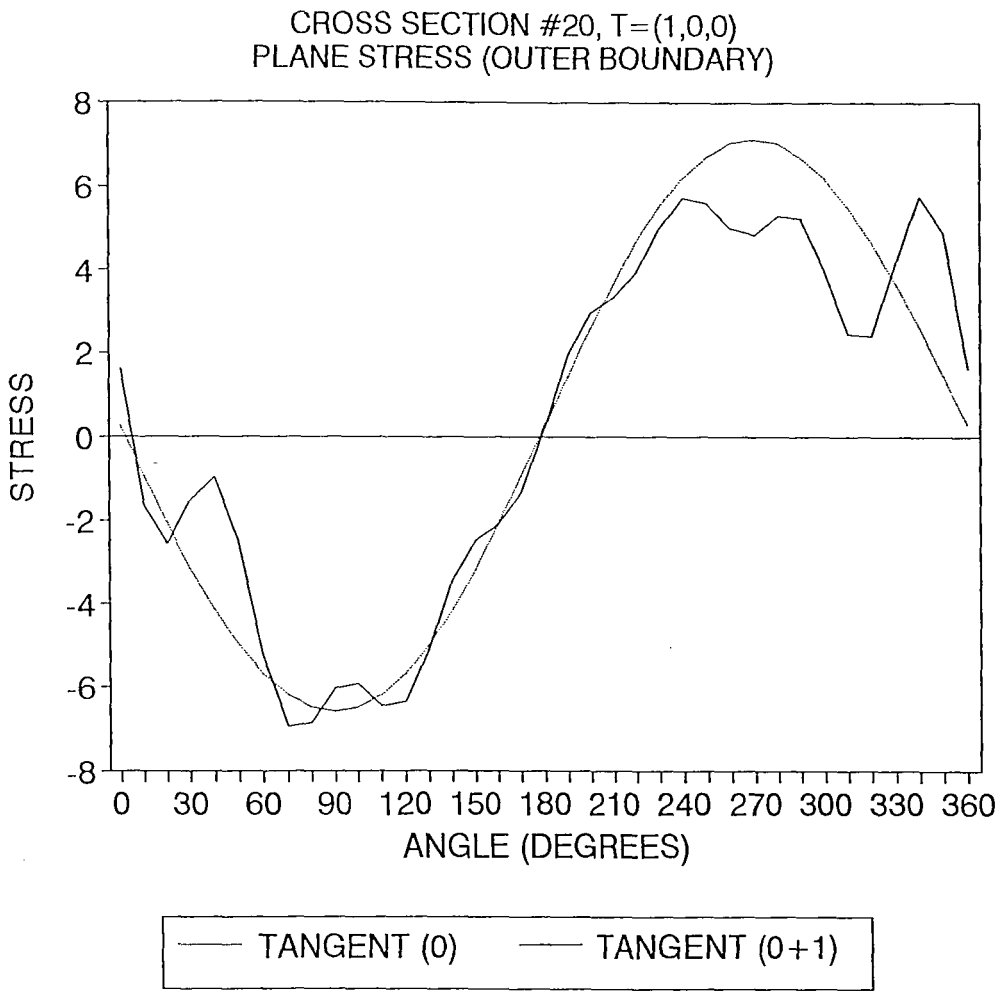
CROSS SECTION #20, T=(1,0,0)
PLANE STRESS (OUTER BOUNDARY)
STRESS
8
6
4
2
0
-2
-4
-6
-8
0 30 60 90 120 150 180 210 240 270 300 330 360
ANGLE (DEGREES)
TANGENT (0)
TANGENT (0+1)

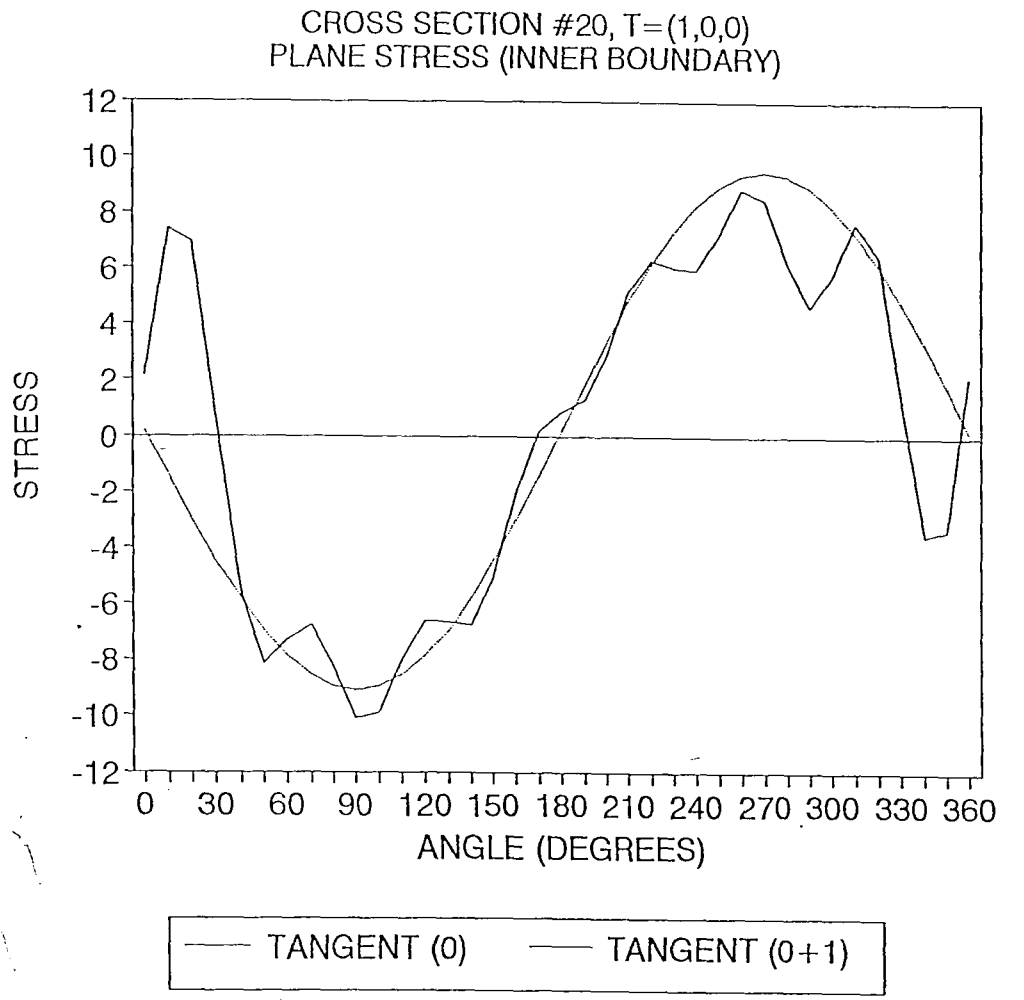
CROSS SECTION #20, T=(1,0,0)
PLANE STRESS (INNER BOUNDARY)
STRESS
12
10
8
6
4
2
0
-2
-4
-6
-8
-10
-12
0 30 60 90 120 150 180 210 240 270 300 330 360
ANGLE (DEGREES)
TANGENT (0)
TANGENT (0+1)

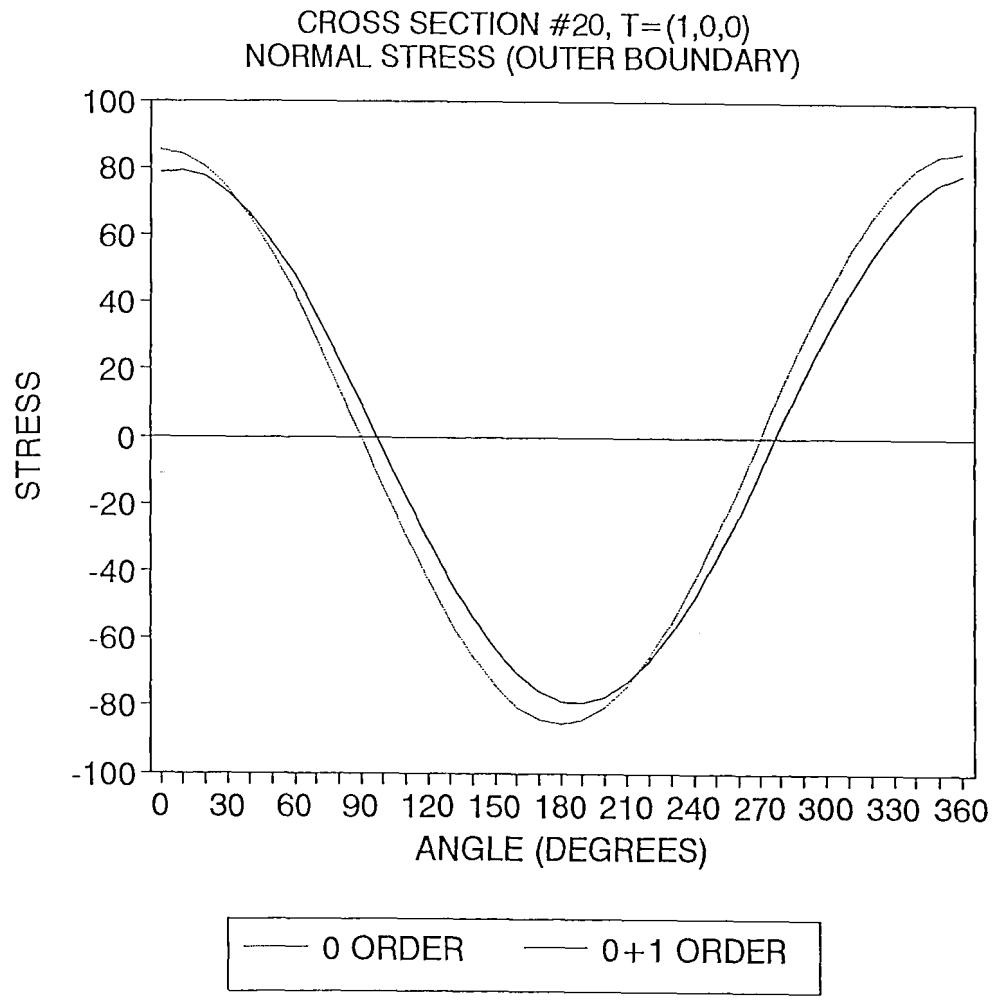
CROSS SECTION #20, T=(1,0,0)
NORMAL STRESS (OUTER BOUNDARY)
STRESS
100
80
60
40
20
0
-20
-40
-60
-80
-100
0 30 60 90 120 150 180 210 240 270 300 330 360
ANGLE (DEGREES)
0 ORDER
0+1 ORDER

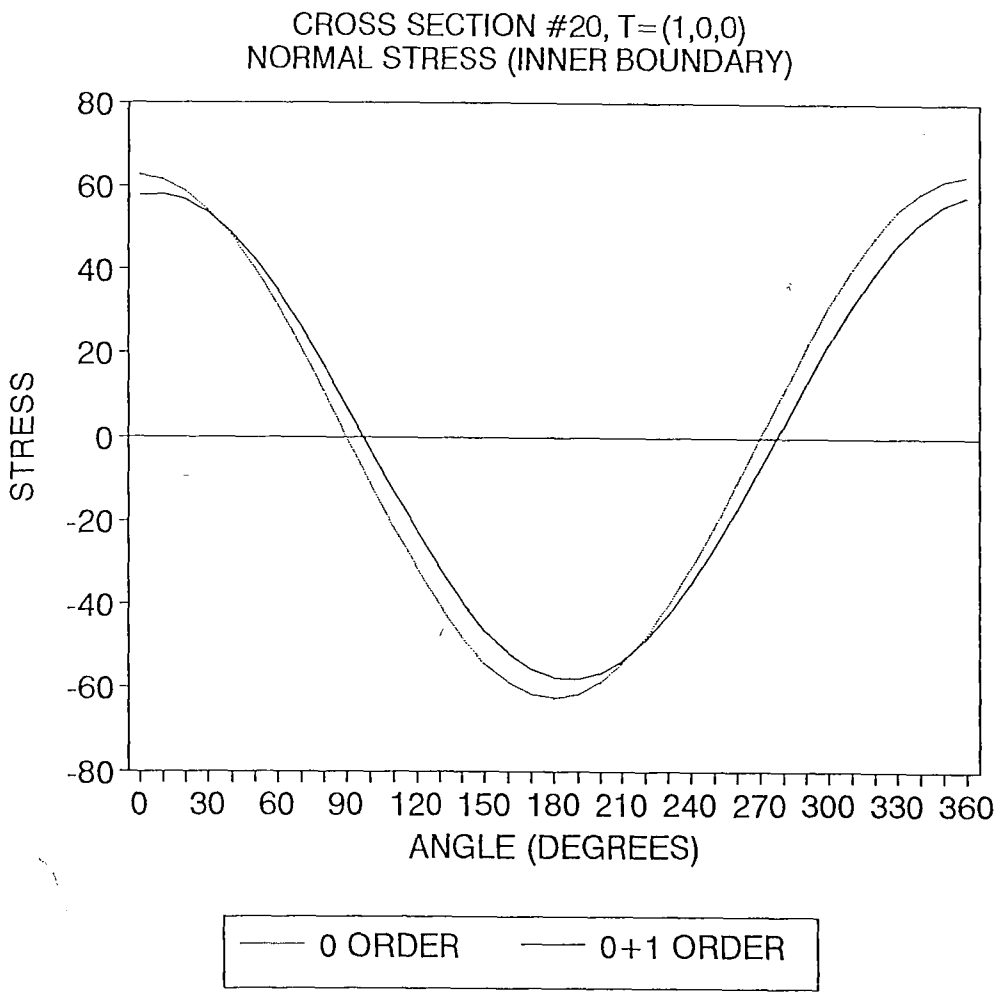
CROSS SECTION #20, T=(1,0,0)
NORMAL STRESS (INNER BOUNDARY)
STRESS
80
60
40
20
0
-20
-40
-60
-80
0 30 60 90 120 150 180 210 240 270 300 330 360
ANGLE (DEGREES)
0 ORDER
0+1 ORDER

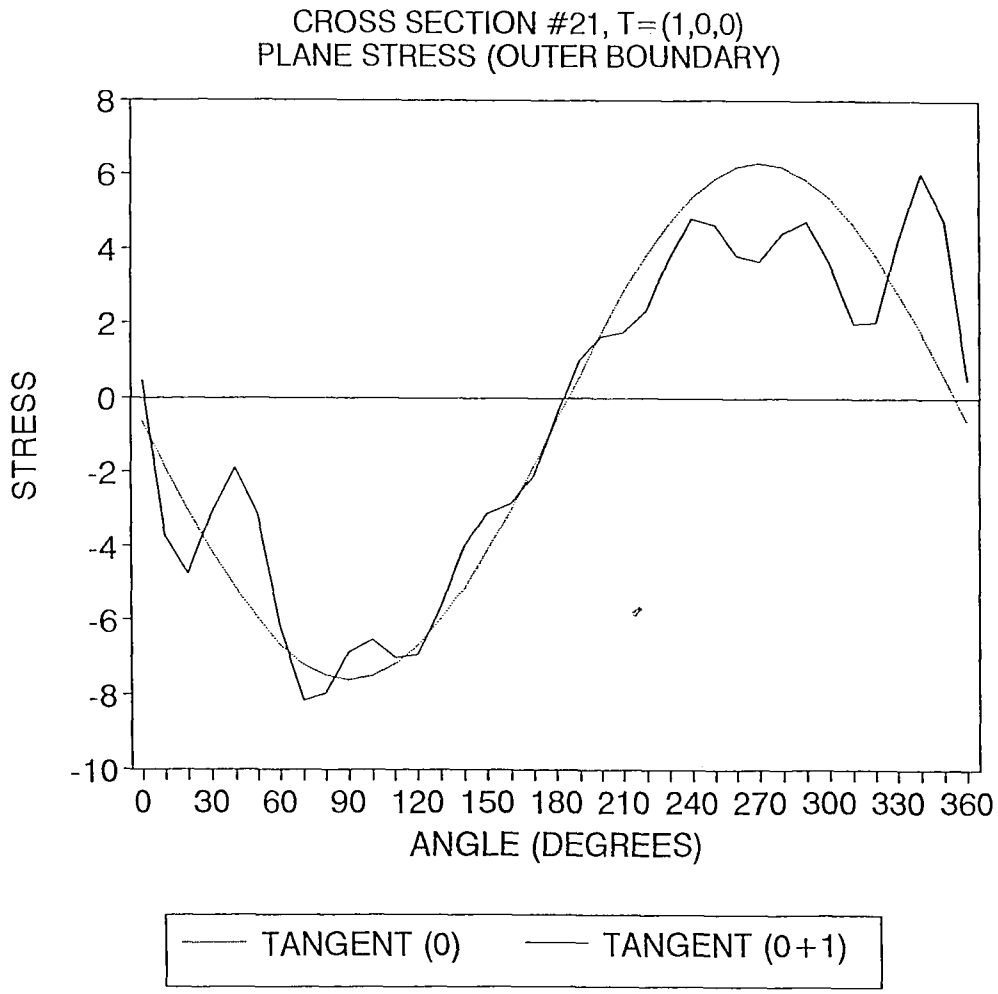
CROSS SECTION #21, T=(1,0,0)
PLANE STRESS (OUTER BOUNDARY)
STRESS
8
6
4
2
0
-2
-4
-6
-8
-10
0 30 60 90 120 150 180 210 240 270 300 330 360
ANGLE (DEGREES)
TANGENT (0)
TANGENT (0+1)

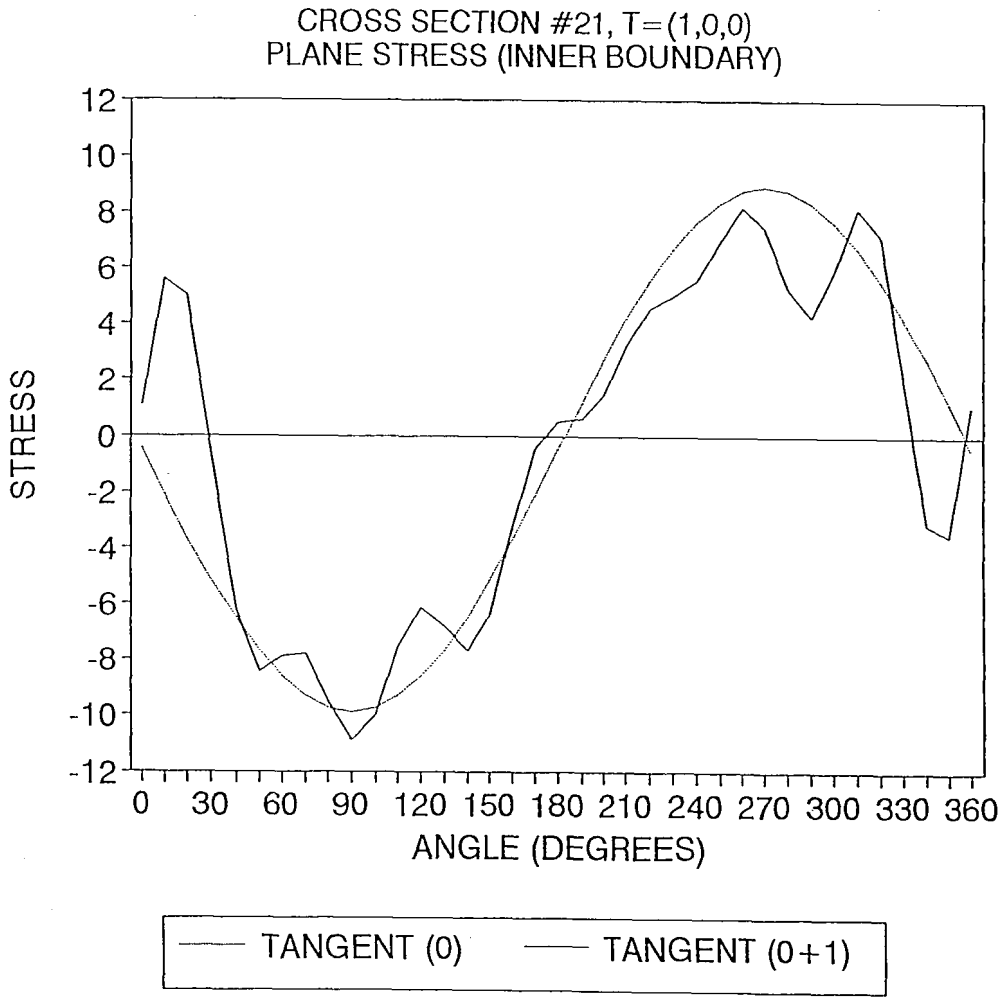
CROSS SECTION #21, T=(1,0,0)
PLANE STRESS (INNER BOUNDARY)
STRESS
12
10
8
6
4
2
0
-2
-4
-6
-8
-10
-12
0 30 60 90 120 150 180 210 240 270 300 330 360
ANGLE (DEGREES)
TANGENT (0)
TANGENT (0+1)

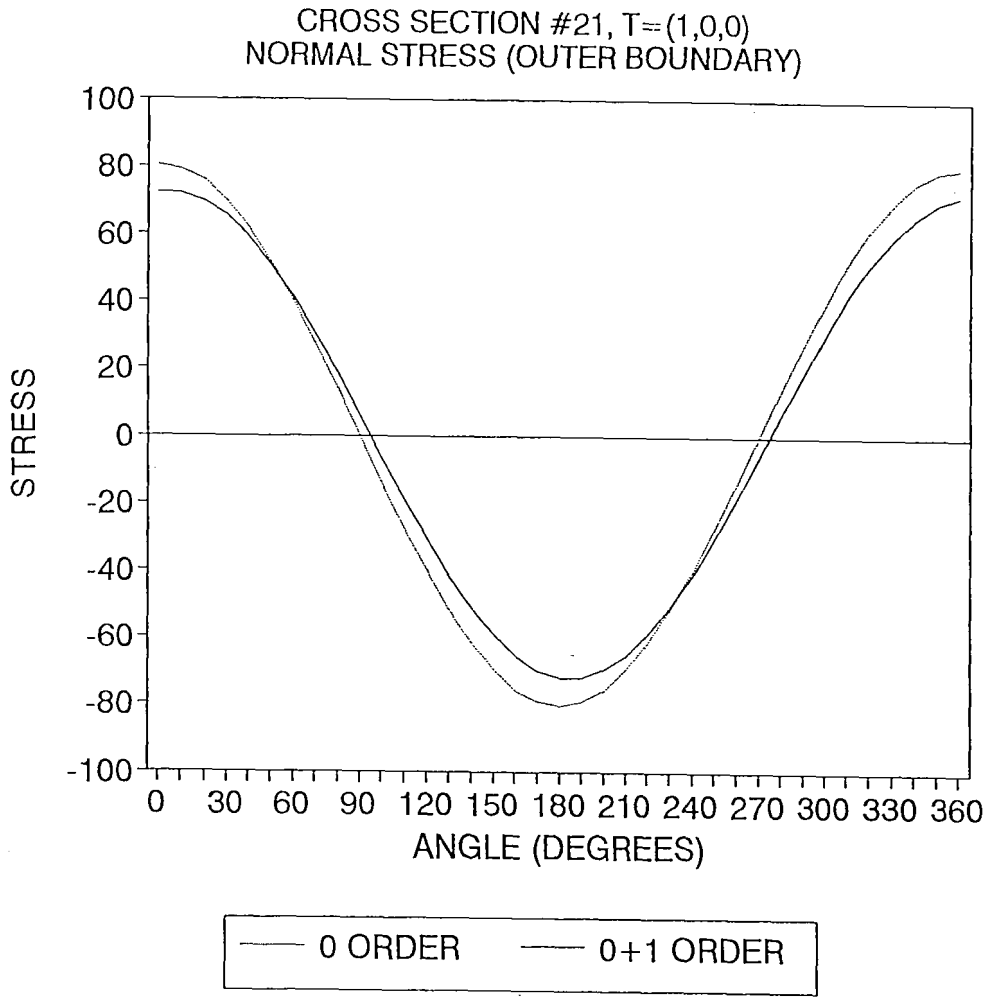
CROSS SECTION #21, T=(1,0,0)
NORMAL STRESS (OUTER BOUNDARY)
STRESS
100
80
60
40
20
0
-20
-40
-60
-80
-100
0 30 60 90 120 150 180 210 240 270 300 330 360
ANGLE (DEGREES)
0 ORDER
0+1 ORDER

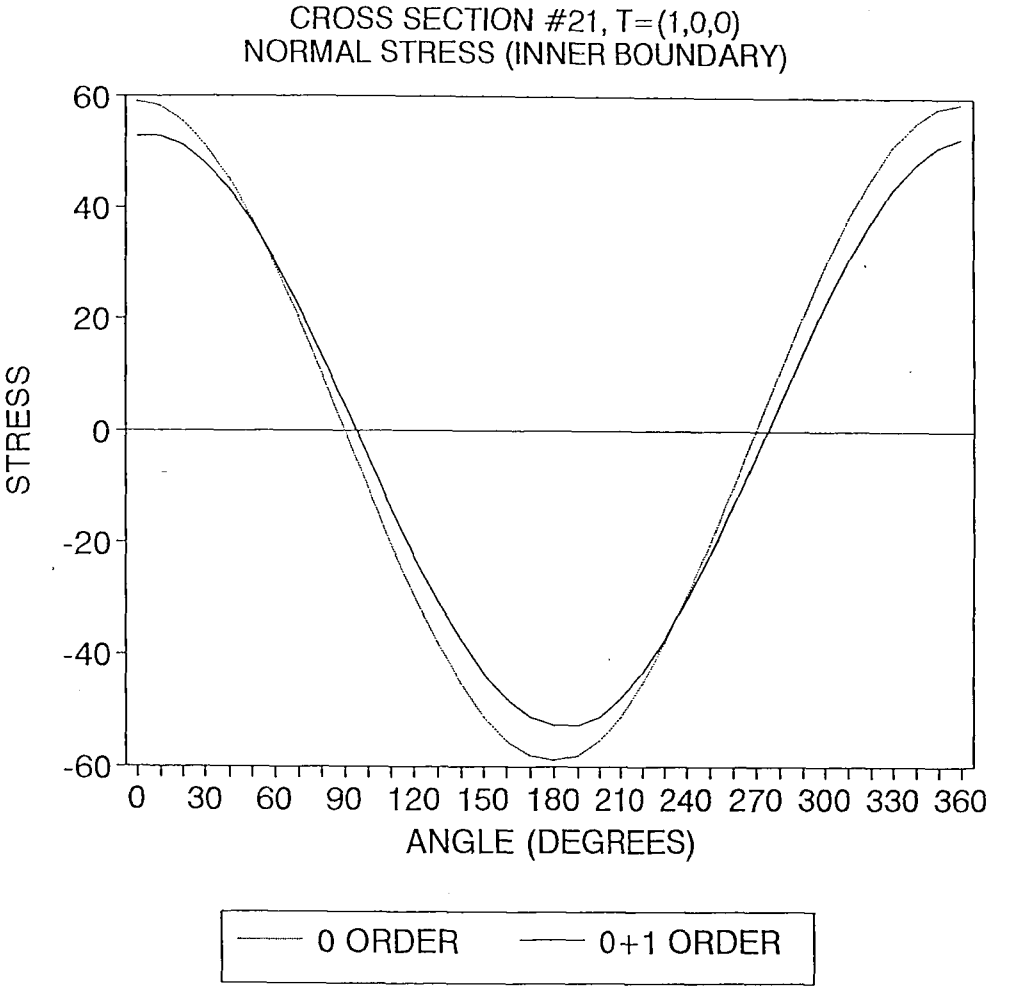
CROSS SECTION #21, T=(1,0,0)
NORMAL STRESS (INNER BOUNDARY)
60
40
20
0
-20
-40
-60
STRESS
0 30 60 90 120 150 180 210 240 270 300 330 360
ANGLE (DEGREES)
0 ORDER
0+1 ORDER

CROSS SECTION #22

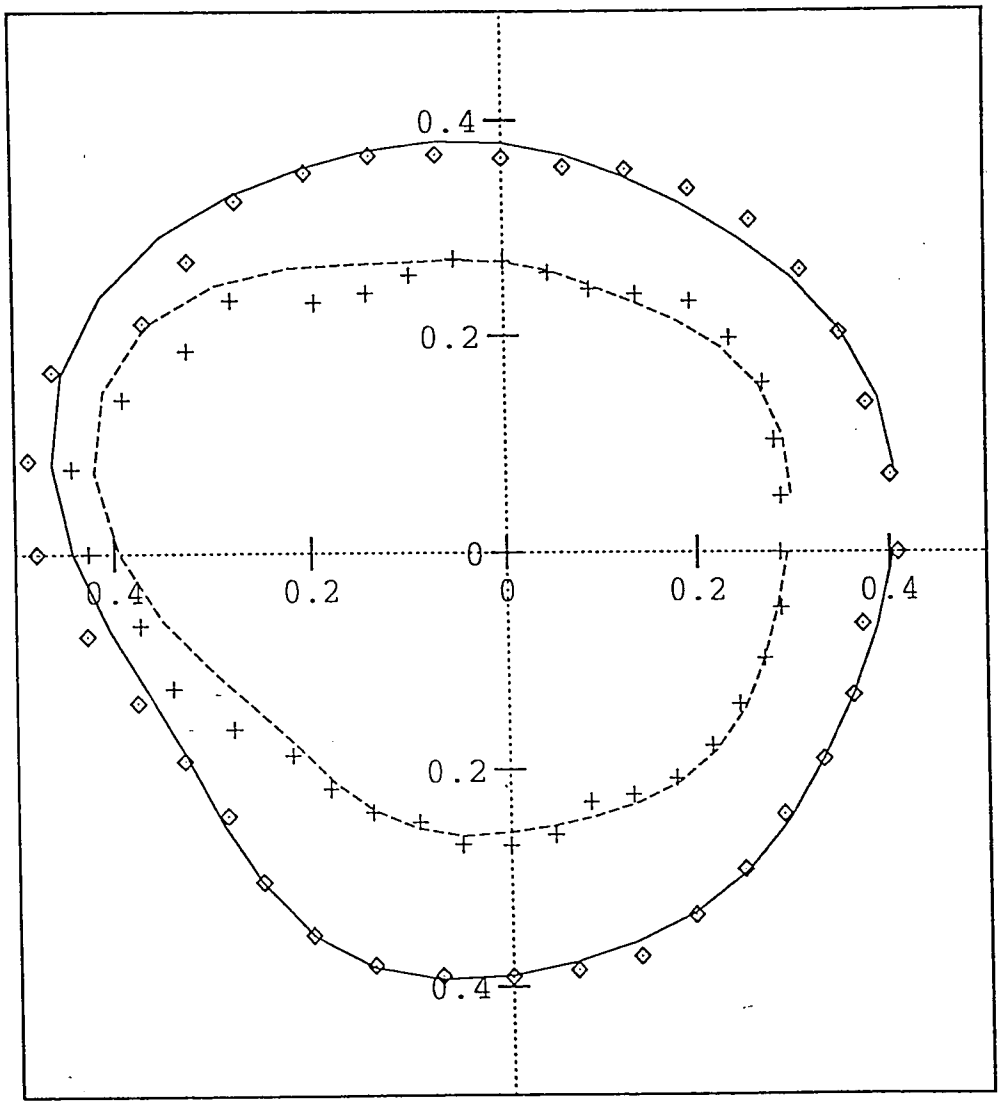

OUTER BDRY ——
INNER BDRY - - - -
ACT OUTER BDRY ◇
ACT INNER BDRY +

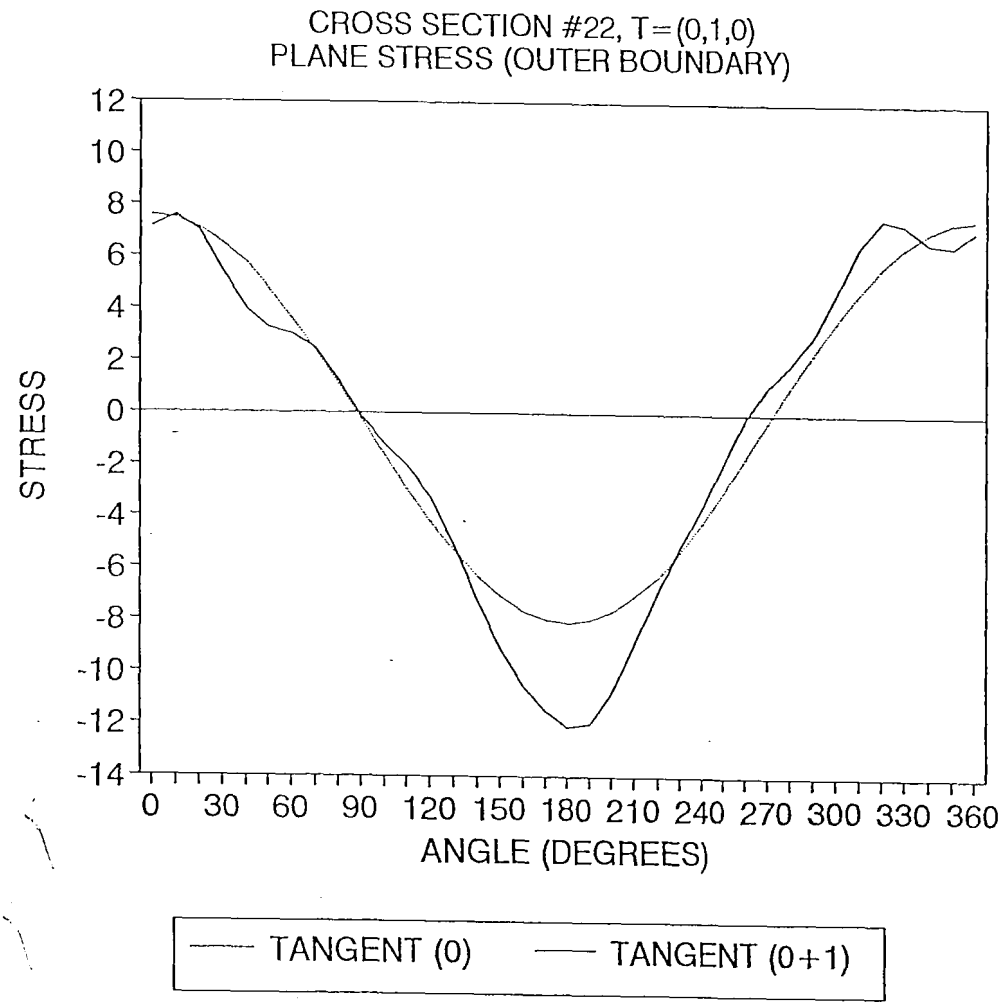
CROSS SECTION #22, T=(0,1,0)
PLANE STRESS (OUTER BOUNDARY)
STRESS
12
10
8
6
4
2
0
-2
-4
-6
-8
-10
-12
-14
0 30 60 90 120 150 180 210 240 270 300 330 360
ANGLE (DEGREES)
TANGENT (0)
TANGENT (0+1)

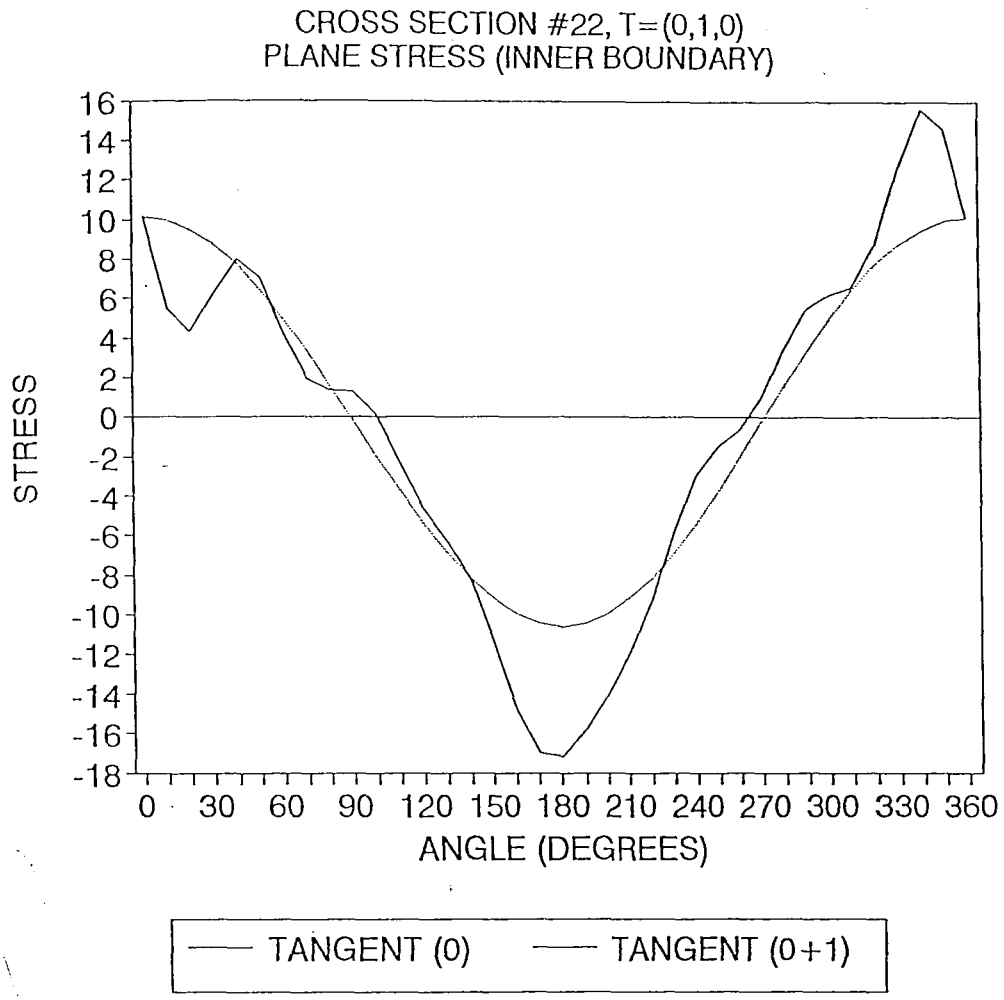
CROSS SECTION #22, T=(0,1,0)
PLANE STRESS (INNER BOUNDARY)
STRESS
16
14
12
10
8
6
4
2
0
-2
-4
-6
-8
-10
-12
-14
-16
-18
0 30 60 90 120 150 180 210 240 270 300 330 360
ANGLE (DEGREES)
TANGENT (0)
TANGENT (0+1)

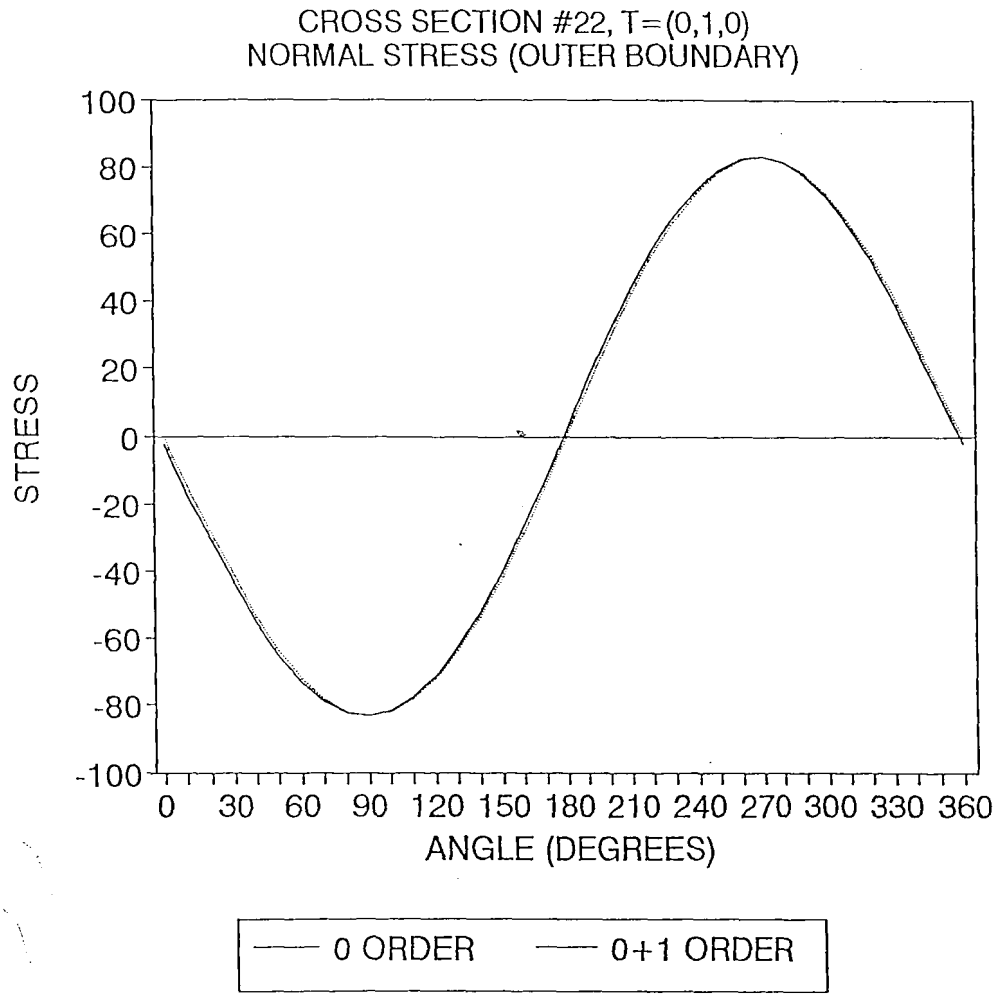
CROSS SECTION #22, T=(0,1,0)
NORMAL STRESS (OUTER BOUNDARY)
STRESS
100
80
60
40
20
0
-20
-40
-60
-80
-100
0 30 60 90 120 150 180 210 240 270 300 330 360
ANGLE (DEGREES)
0 ORDER
0+1 ORDER

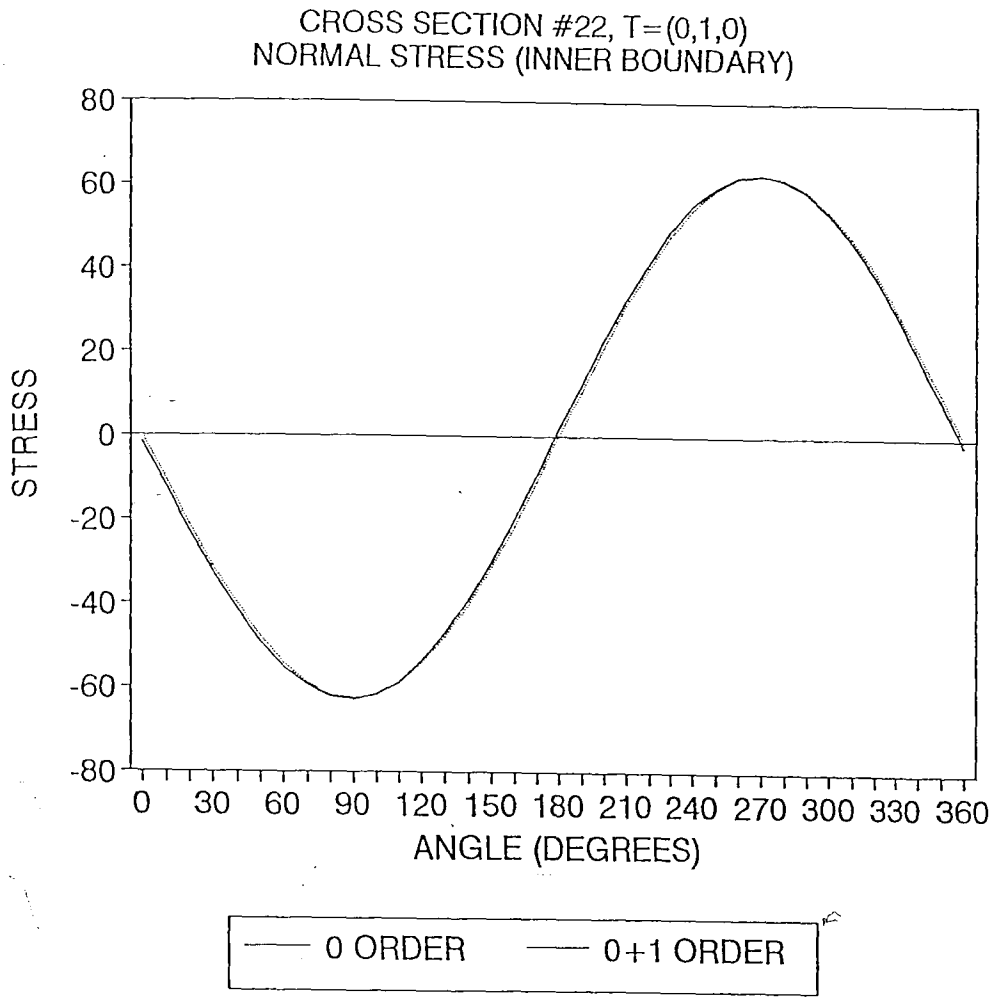
CROSS SECTION #22, T=(0,1,0)
NORMAL STRESS (INNER BOUNDARY)
STRESS
80
60
40
20
0
-20
-40
-60
-80
0 30 60 90 120 150 180 210 240 270 300 330 360
ANGLE (DEGREES)
0 ORDER
0+1 ORDER

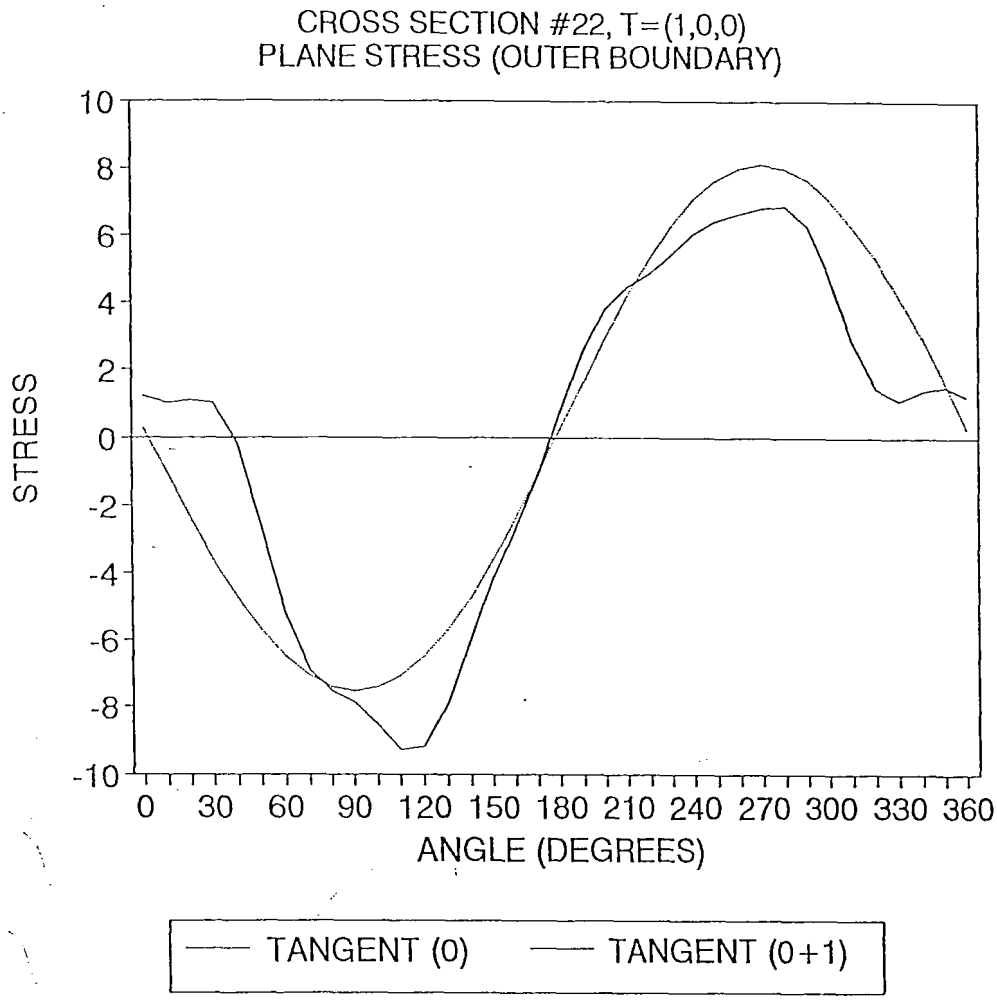
CROSS SECTION #22, T=(1,0,0)
PLANE STRESS (OUTER BOUNDARY)
STRESS
10
8
6
4
2
0
-2
-4
-6
-8
-10
0 30 60 90 120 150 180 210 240 270 300 330 360
ANGLE (DEGREES)
TANGENT (0)
TANGENT (0+1)

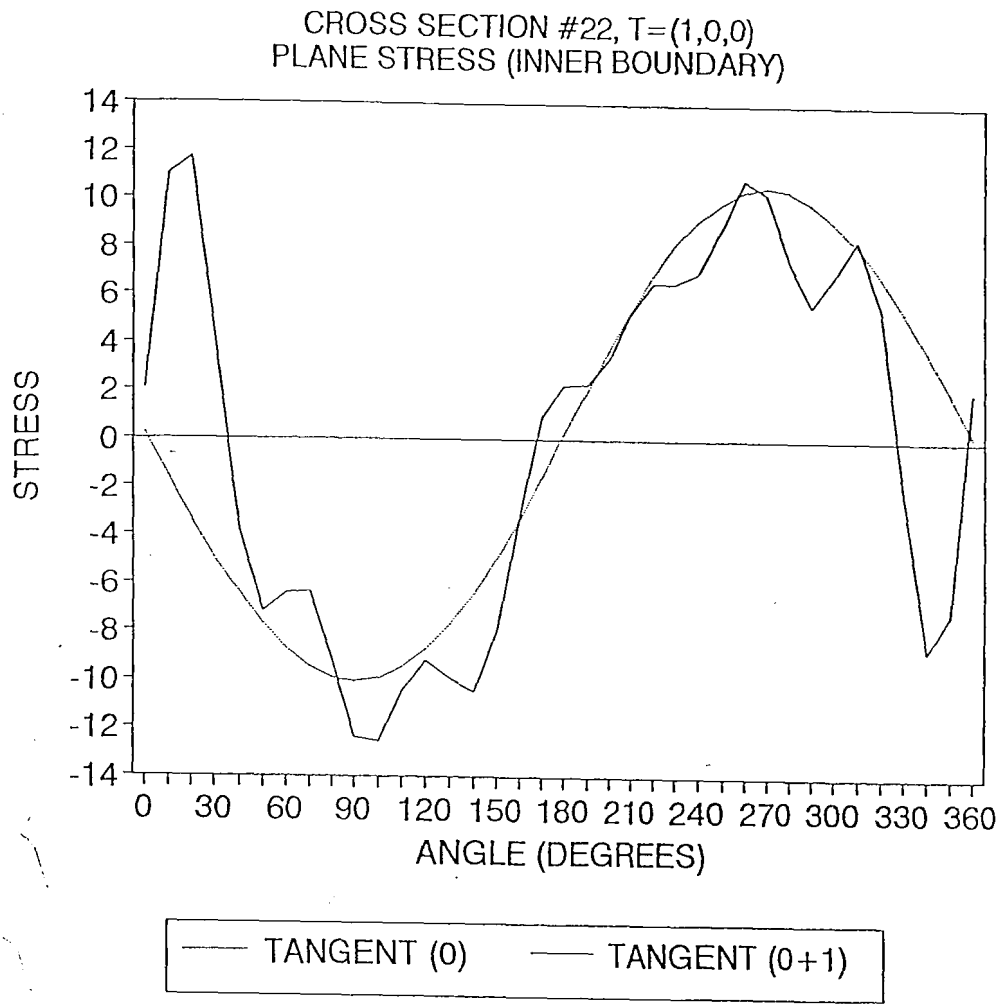
CROSS SECTION #22, T=(1,0,0)
PLANE STRESS (INNER BOUNDARY)
STRESS
14
12
10
8
6
4
2
0
-2
-4
-6
-8
-10
-12
-14
0 30 60 90 120 150 180 210 240 270 300 330 360
ANGLE (DEGREES)
TANGENT (0)
TANGENT (0+1)

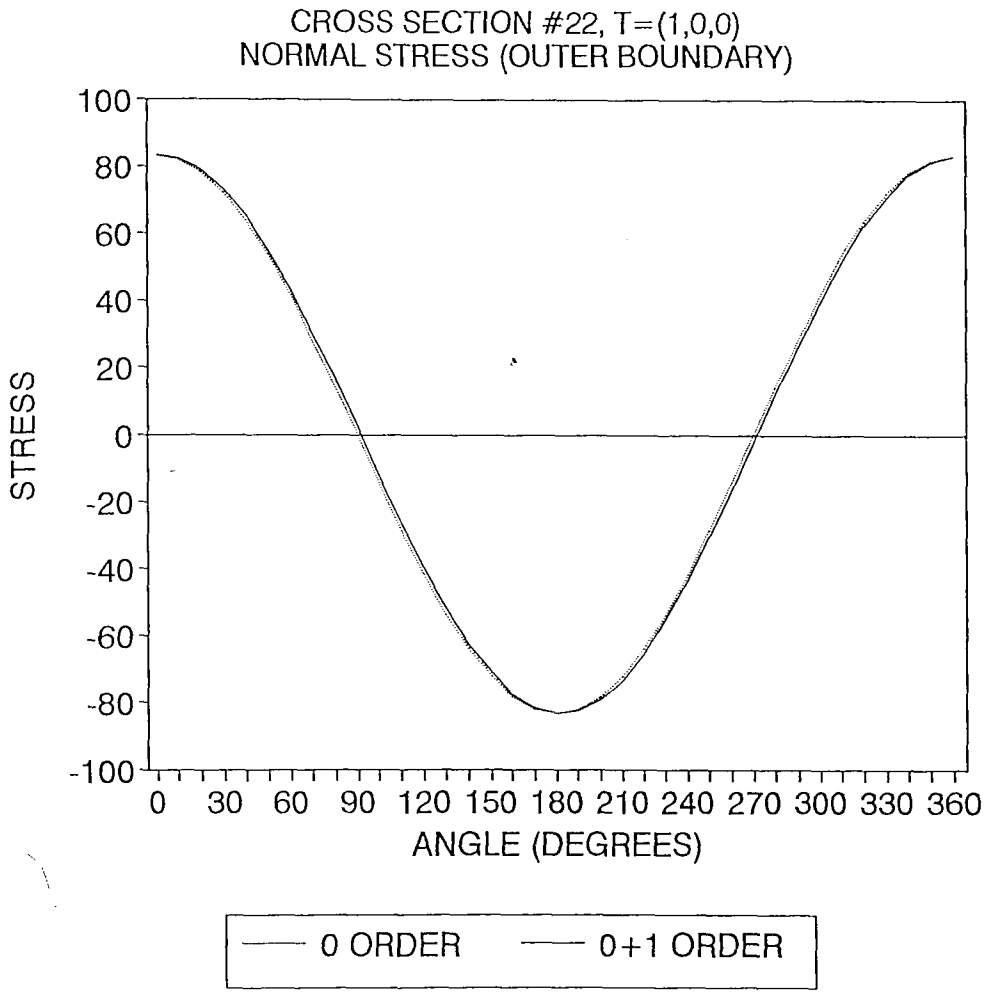
CROSS SECTION #22, T=(1,0,0)
NORMAL STRESS (OUTER BOUNDARY)
STRESS
100
80
60
40
20
0
-20
-40
-60
-80
-100
0 30 60 90 120 150 180 210 240 270 300 330 360
ANGLE (DEGREES)
0 ORDER
0+1 ORDER

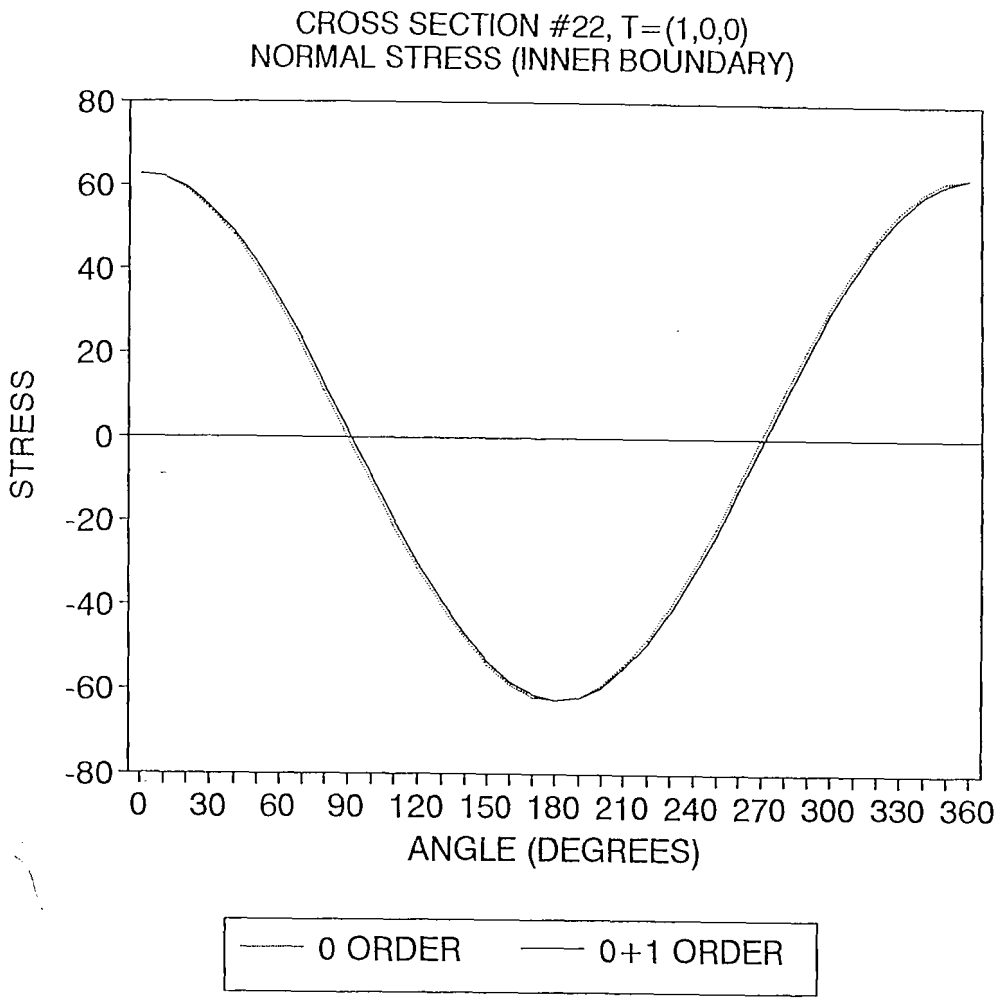
CROSS SECTION #22, T=(1,0,0)
NORMAL STRESS (INNER BOUNDARY)
STRESS
80
60
40
20
0
-20
-40
-60
-80
0 30 60 90 120 150 180 210 240 270 300 330 360
ANGLE (DEGREES)
0 ORDER
0+1 ORDER

Vita

Sean A. McIntyre was born in Easton, Pennsylvania on March 3, 1968. His parents are Barrie and Barbara McIntyre. He received his B.S. degree from Moravian College, located in Bethlehem, PA, in 1990. He is a member of Pi Mu Epsilon, a national mathematics honors fraternity. He has two sisters, Heidi McIntyre and Heather Pesche. He has a brother-in-law, David Pesche, and a niece, Jordan Pesche.

END

OF

TITLE